THESIS

RADAR AND LIGHTNING ANALYSES OF GIGANTIC JET-PRODUCING STORMS

Submitted by

Tiffany C. Meyer

Department of Atmospheric Science

In partial fulfillment of the requirements

For the Degree of Master of Science

Colorado State University

Fort Collins, Colorado

Fall 2012

Master's Committee:

Advisor: Steven A. Rutledge

Raymond Robinson
Russ Schumacher
Timothy Lang

ABSTRACT

RADAR AND LIGHTNING ANALYSES OF GIGANTIC
JET-PRODUCING STORMS

An analysis of the storm structure and evolution associated with six gigantic jets was conducted. Three of these gigantic jets were observed within detection range of very high-frequency lightning mapping networks. All six were within range of operational radars and two-dimensional lightning network coverage: five within the National Lightning Detection Network and one within the Global Lighting Detection network. Most of the storms producing the jets formed in a high CAPE, low lifted index environments and had maximum reflectivity values of 54 to 62 dBZ and 10-dBZ echo tops reaching 14-17 km. Most storms were near the highest lighting flash rate and peak storm intensity with an overshooting echo top just before or after the time of the jet. The overshooting top and strong intensification may have indicated a convective surge which allowed the upper positive charge to mix with a negatively charged screening layer that became depleted. Intra-cloud lightning initiating in the mid-level negative region could have exited upward through the recently depleted positive region, producing a gigantic jet.

ACKNOWLEDGEMENTS

This work was made possible due to the support of various individuals and organizations. I would like to deeply thank my advisor, Dr. Steven A. Rutledge, for his guidance and support throughout this study. Especially in the past couple months that I have been working remotely due to a new job. I would also like to extend my gratitude to Dr. Steven Robinson, Dr. Russ Schumacher, and Dr. Timothy Lang for serving in my committee and providing highly useful feedback. Furthermore, I am very grateful for the advice of Dr. Walt Lyons, who provided invaluable instruction on the history and formation of gigantic jets. I also want to thank Vaisala, Inc. for providing the NLDN and GLD360 data used in this study. Without the observations of the gigantic jets, this study would not have been possible. The GJs were observed by Joel Gonzalez in Florida, by Kevin Palivec in Texas, and by Frankie Lucena in Puerto Rico. I am greatly appreciative of the faculty and my colleagues at the Colorado State University Department of Atmospheric Science for aiding in my education understanding of meteorology. I would specially like to thank the Rutledge research group for always helping me when needed, particularly when I was needing help with the physics background associated with lightning and gridding of radar data. I am also very grateful for my family and friends for their strong support throughout my education journey. In addition, this study would not have been possible without the financial support of the DARPA NIMBUS program.

TABLE OF CONTENTS

1. Introduction

1.1 Global Electric Circuit

The global electric circuit (GEC) describes an electrical current flowing between the highly conducting ionosphere and the Earth's surface forming a giant spherical condenser [*Lakhina*, 1993; *Bering III*, 1995; *Bering III et al.*, 1998; *Rycroft et al*., 2000; *Siingh et al.*, 2005]. A downward directed electric field exists in this cavity. This circuit is charged by thunderstorms to a potential of several hundred thousand volts [*Roble and Tzur* 1986]. The downward electric field on a clear day is 100 to 300 volts/meter at the Earth's surface. William Thomson [1860] purposed that the ionosphere is charged to a potential of about 260 kV as a positive plate compared to the Earth's surface, a negative plate. There are three quasi-direct current sources that drive the global circuit: thunderstorms, the dynamo interaction between solar wind and magnetosphere, and the dynamo effect of atmospheric tides in the thermosphere [*Roble,* 1991]. Roble suggests that thunderstorms are the most powerful of the three sources. The Wilson current states the electric current flows upward through thunderstorms into the ionosphere where it spreads out over the globe through the ionosphere and magnetosphere. The current returns to the Earth as the fair-weather air-Earth current. Negative cloud-to-ground (CG) lightning returns the charge to the thunderstorm and closes the global circuit [*Bering III et al.*, 1998]. Figure 1 shows the flow of the electric current in the global circuit.

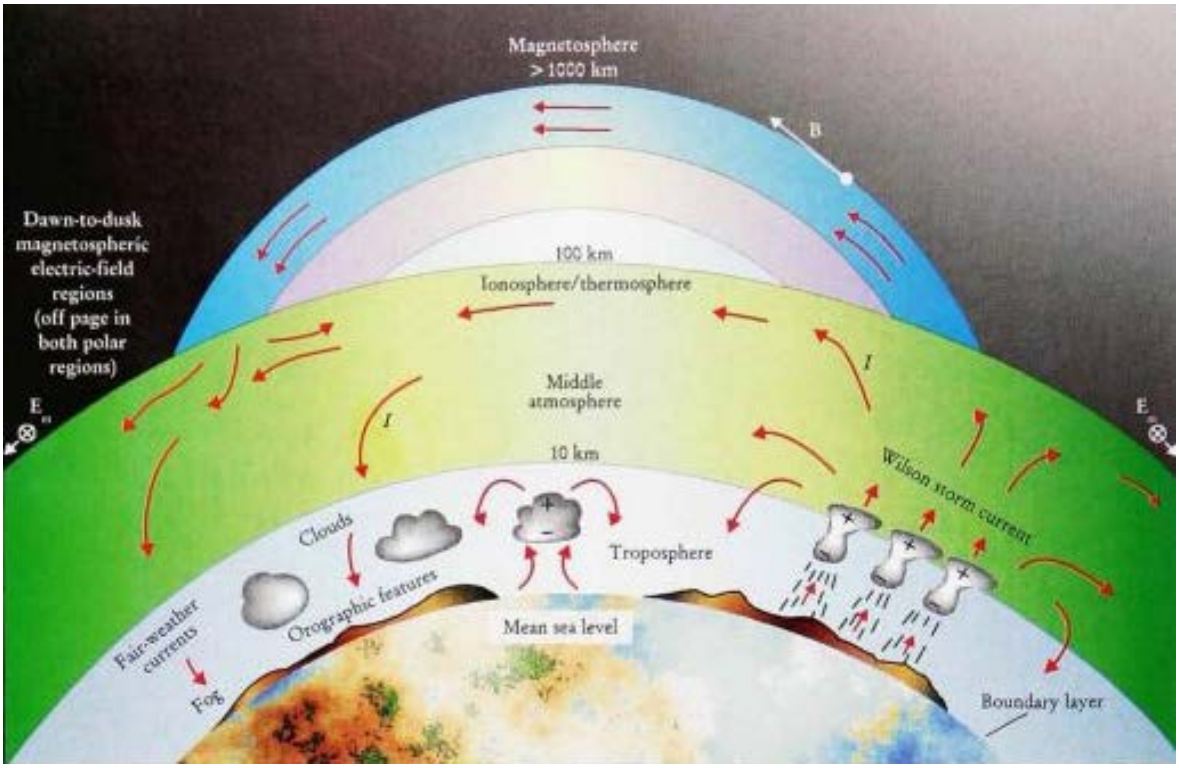

Figure 1. Flow of electric current in the global circuit. All of the unlabeled arrows represent current flow. The strongest batteries in the circuit are the thunderstorms indicated on the right. They produce the Wilson current. The fair-weather currents are indicated by downward-pointing arrows away from the thunderstorms. (Based on a diagram by Bering III et. Al 1998).

1.2 Charge Structure

Lightning activity can give insight into storm charge structure. Traditionally the conceptual model of the gross electrical structure of thunderstorms is that it can be described as either dipolar or tripolar where the main charges are a middle-level negative charge and an upper-level positive charge [*Kulman et al.*2006]. Sometimes a positive charge can be found below the negative charge to form a tripole structure [*Williams et al.* 1989]. In the lower region rain and water droplets make up this positive charge while the upper positive region is due to ice crystals. Graupel and hail carry a negative charge and are located in the mid-level regions.

A screening layer of negative charge has also been found to form on the top boundary of the cloud. The formation of this charge layer does not depend on hydrometeors being polarized by the electric field, so it is classified as a noninductive, ion-particle mechanism. For the

thunderstorm to maintain a constant current across the boundary (equilibrium), the layer of charge increases the thunderstorm electric field just inside the boundary and decreases it outside the boundary to compensate for the discontinuity in conductivity. Since the layer of charge reduces the electric field outside the storm, it is called a screening layer [*MacGorman and Rust* 1998].

While most storms are normal polarity, as explained above, so called "inverted storms do occur. In these cases the upper region is dominated by negative charge and the middle region dominated by positive charge. One main difference of the reversed or inverted polarity storms is that the storms are usually dominated by flashes that lower positive charge to the ground instead of the usual negative charge. [*MacGorman et al.,* 2008]. Inverted storms are often severe [*Carey et al.,* 2003]

1.3 Previous GJ Studies

All lightning including the normal CG and intracloud (IC) lightning as well as the more uncommon transient luminous events (TLEs) play a role in the GEC. Gigantic jets (GJs) are part of the TLE family. Like blue jets they are thought to initiate from intracloud (IC) lightning and escape upward from cloud tops. GJs extend to higher altitude than blue jets, up to 70-90 km, and have a different appearance [*Pasko and George,* 2002; *Su et al*. 2003; *Lyons et al.*, 2003]. Blue jets are thought of as a positive discharge resembling a continuous positive leader-like propagation [*Wescott et al.*, 2001; 1998]. Gigantic jets have an impulsive re-brightening characteristic resembling negative leader processes [*Krehbiel et al.,* 2008].

The first GJ was observed in 2001. On 14 September the Lidar Laboratory of Arecibo Observatory, Puerto Rico observed a GJ reaching ~70 km off the northwest coast of Puerto Rico

from the main core of a relatively small thunderstorm that had a cloud top of about 16 km [*Pasko et al.,* 2002]. In July 2002 low-light-level cameras in Kenting, Taiwan recorded five GJs above a 16 km tall thunderstorm over the South China Sea ranging in height from 86-91 km [*Su et al.*, 2003]. Two years later, a GJ was recorded in a frontal system over Anhui province of China. This observation proved gigantic jets could also occur over land. A few months later several jet-like TLEs were recorded over a thunderstorm on the coast of Guandong province, China [*Hsu et al*., 2004]. Two low-light cameras near Marfa, Texas recorded the first gigantic jet over North America on 13 May 2005. The likely parent thunderstorm was a high-precipitation supercell cluster with radar echo tops of at least 14 km. This was a negative GJ that was believed to have occurred in an inverted tripole charge configuration due to a rapid rise of +CG flash rates and a 5-minute period with almost no –CG flashes just before the GJ. However, charge configurations can be complex and are subject to intense study [*Van der Velde et al.*, 2007a]. Since then, more GJs have been recorded in North America [*van der Velde et al.,* 2007a,b]. The first positive jet was observed just west of Corsica (Europe) the night of 12 December 2009. A stationary Mediterranean winter thunderstorm with a cloud top of only 6.5 km produced this GJ. The positive polarity was confirmed by the electromagnetic waveforms of various radio receiver stations [*van der Velde et al.,* 2010]. In 2010, three GJs were optically detected in different storms within detection range of ground-based, very high frequency (VHF) networks that resolve three-dimensional (3D) lightning development. *Lu et al.* [2011b] examined two of these jets and indicated that lightning development associated with these negative GJs is remarkably similar in that both jets initiated from convective cells that were producing normal-polarity IC lightning between mid-level negative and upper positive charge regions. The GJs were produced by lightning flashes that developed as if there were a depleted upper positive charge region, as

suggest by *Krehbiel et al*. [2008]. Specifically one of the jets (from Florida) was initiated by a narrow bipolar event (NBE). This initiating NBE radiated the largest low frequency (LF) impulse of the flash and was detected by the National Lightning Detection Network as having a +56-kA peak current. The jet ascended at a velocity of ~500 km/s to 80 km in altitude and had accumulated a charge moment change of +8000 C-km, or removal of an estimated 110 C of negative charge from a cloud region if all the charge was deposited at 80 km altitude. Charge moment change is defined as the product of the charge amount and the altitude from which the charge is lowered. Another of the jets (from Oklahoma) reached an overall upward propagation speed of only ~270 km/s while reaching 90 km in altitude. Only 10-20 C of overall negative charge was transferred to the ionosphere, five times less than the Florida GJ, but neither had significantly discharged an extensive negative region of cloud [*Lu et al.*, 2011b]. The Table 1 shows a list of ground-based GJs observed and some of the storm characteristics. Overall, 24 GJs have been recorded in storms with deep convection, >14 km echo tops and ~55 dBZ reflectivity cores. Continued observations are being taken to capture more GJs in hopes to better understand them.

Table 1. Ground-based gigantic jet observations. Highlighted in grey are the cases looked at in this study.

Date	Place	L/W	Storm Type	Cloud Top (km)	Jet Height (km)	Reference	Notes
15 Sep 2001	200 km NW of Puerto Rico	Water	Thunderstorm Cell	16	70	Pasko et al., 2002	
22 Jul 2002	~500 km SSW of Kenting, Taiwan	Water	Thunderstorm Cell	16	86-91	Su et al., 2003	5 events between 1409 and 1421 UTC
18 Jun 2004	~700 km from Anhui province of China	Land	Frontal System	?	?	Hsu et al., 2004	
3 Aug 2004	~500 km from Guandong province, China	Coast	Thunderstorm Cell	?	70	Hsu et al., 2004	Possible gigantic jet
13 May 2005	Northern Mexico	Land	HP Supercell	14	69-80	van der Velde et al., 2007a	
20 Aug 2007	Missouri	Land	Quasi-supercell	15-16	?	van der Velde et al., 2007b	Produced 2 jets and a sprite
21 Jul 2008	Off coast near Duke	Water	TS Cristobal	15	88	Cummer et al., 2009	
8 May 2009	Off coast near Duke	Water	Isolated cell				
12 Dec 2009	West of Corsica	Land	Stationary winter thunderstorm	6.5	91	Van der Velde et al., 2009	First +GJ produced ~50 TLEs
7 March 2010	East of Reunion Island	Water	Isolated tropical storm	?	80-90	Soula et al., 2011	5 events between 1740 and 1829 UTC
9 Sep 2010	Eastern OK	Land	TS Hermine	15	90	Lu et al., 2011b	2 events in 10 minutes
28 Sep 2010	205 km from Sebring, FL	Water	Convective Cell (Remnants of TS)	16.2	80	Lu et al., 2011b	First jet to ascend into daytime ionosphere
17 Apr 2011	NC	Water	Squall line supercell	15	?	Lu et al., 2011a	Positive GJ
22 Sep 2011	Puerto Rico	Land	Convective cell in a tropical airmass	15	?	Lyons (2012)* URSI talk	

1.4 Upward Lightning Formation

The formation of CG and IC lightning are reasonably well understood, however blue jet and gigantic jet formation is still not fully understood. *Krehbiel et al.* [2008] offered a theory as to how upward electrical discharges form from thunderstorms. In a normal electrified thunderstorm the electrical structure consists of a mid-level negative region with upper and lower positive charge regions and a negative screening layer around the upper cloud boundary [*Krehbiel,* 1986; *Williams,* 1989]. As the storm charges and the electric fields build up from precipitation, discharges occur producing different types of lightning. Normally electrified storms tend to develop an overall negative charge imbalance with time as a result of the negative screening charge flowing to the cloud top [*Wilson,* 1921]. A –CG discharge occurs when a breakdown is triggered between the mid-level negative and lower positive charges and escapes out of the storm downward [*Marshall et al.,* 2005] charging the global electric circuit. After a –CG discharge the storm's net charge becomes positive and the electric field is enhanced in the upper part of the storm [*Wilson,* 1956]. As the storm continues to charge, a discharge can be triggered in the upper part of the storm that would be expected to escape upwards. The upward discharge would have the same polarity as the storm, namely positive for a normally electrified storm. If mixing of the screening layer and upper positive charge layer is weak or absent, upward discharges are predicted to commonly occur; but since jets are not very common, this suggests the mixing of the screening charge is normally strong [*Krehbiel et al.,* 2008]. These upward discharges are known as blue jets.

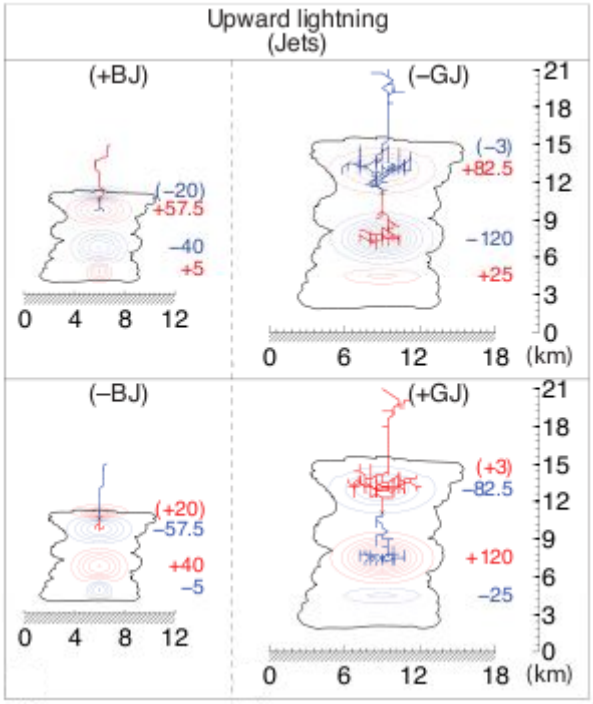

Figure 2. Illustrative lightning simulations for normal- and inverted-polarity storms, showing the four possible types of upward discharges, classified by initiation mechanism (blue jet and gigantic jet) and upward polarity (+ and \u2212). Blue and red contours and numbers indicate negative and positive charge regions and charge amounts (in C), respectively, each assumed to have a Gaussian spatial distribution. Blue jets will tend to be initiated by a precursor discharge (either CG or IC) that causes a charge imbalance in the storm [Riousset et al., 2010; Krehbiel et al., 2008, Supplementary Information].

Krehbiel et al. [2008] suggest a secondary mechanism for the formation of upward discharges which may explain their occurrence. For a negative GJ to be produced by a normally electrified storm, it would need to originate in the mid-level negative storm charge. In the case of a bolt-from-the-blue (BFB), discharges begin as regular, upward-developing IC flashes and a breakdown occurs allowing the leader to be of negative polarity resulting in a CG stoke that lowers negative charge to the ground. This leaves a charge imbalance where the upper positive charge is depleted and is able to mix with the screening charge. As the BFB exits the cloud and turns toward the ground it is "guided" by inferred positive screening charge attracted to the lateral cloud boundaries by the mid-level negative charge [*Krehbiel et al.*, 2008]. In the case of a negative gigantic jet, there is no "guiding" so the preferred discharge mode of the IC flash with a depleted upper positive charge is upward. Blue jets contribute to charging the global electric

circuit whereas negative GJs discharge the circuit by up to 30 C of charge [*Su et al.*, 2003]. For the case of an inverted electrified storm a negative blue jet or positive gigantic jet could be produced. Figure 2 shows the cloud charge structure for the positive and negative cases of upward lightning.

1.5 Overview

In this study six gigantic jets are looked at. Three negative GJs occurred within 3-D lightning mapping arrays (LMAs): two in Oklahoma and one in Florida. *Lu et al.* [2011b] looked at one of the Oklahoma jets and the Florida GJ. A fourth negative jet in Puerto Rico, a negative jet off the coast of North Carolina and a positive jet also off the coast of North Carolina were analyzed. This is only the second positive jet to be recorded. The last three jets were not within a 3D VHF lightning mapping rang, but two-dimensional lightning data were analyzed. An analysis of the meteorological environment and 3D storm structure was performed for all six GJs.

2. Data and Methodology

Lightning, radar, and sounding data was used to analyze the gigantic jets in this study. Two different ground based lightning networks were used as well as two VHF LMAs. For each storm data from the closest radar was obtained. For each case the sounding profile at the time just before the jet and location closest to the location was analyzed. Since the jets can only be recorded via low-light high-speed cameras they are only seen at night as a contrast to the dark sky, therefore satellite data is not useful.

2.1 2-Dimensional Lightning Networks

2.1.1 National Lightning Detection Network

The National Lightning Detection Network (NLDN) has been detecting the electromagnetic radiation from lightning return strokes and providing detailed lightning data for the entire continental United States since 1989 [*Orville,* 2008]. Up until 2006, only CG lightning flashes were detected by the NLDN, however previous studies had shown that severe storms produce much higher rates of IC lightning than CG [*MacGorman and Nielson,*1991; *Weins et al.,* 2005; *Williams et al.,* 1999]. In the early 2000's Vaisala Inc. took over the NLDN and the 100+ sensors were modified to allow the detection of large-amplitude very low frequency (VLF)/LF pulses in the form of cloud flashes [*Cummins and Murphy,* 2009]. During this time the Improved Accuracy from Combined Technology (IMPACT) sensor was developed to combine the time of arrival and direction finder technologies [*Orville,* 2008]. Currently 47 sites have the IMPACT sensor and 59 have the upgraded lightning position and tracking system (LPATS-III) sensors [*Cummins et al.,* 1998]. Lightning information on location, amplitude (peak current), and polarity are recorded for each stroke within a flash. A flash is defined by Cummins and Murphy [2009] as the ensemble of all CG strokes that strike within 10 km of each other within a 1-s

interval. NLDN is the most accurate and reliable large-scale detection network in the world with a detection efficiency of 95% and location accuracy up to 500 m [*Vaisala Inc.,* 2011]

2.1.2 Global Lightning Dataset 360

In 2009, Vaisala's Global Lightning Dataset (GLD360) was launched as the first ground-based lightning detection network capable of providing worldwide coverage. The network consists of VLF long-range sensors. Lightning discharge produces an impulsive electromagnetic wave that propagates through the Earth-ionosphere waveguide and geo-location is then achieved by comparing measurements of radio atmospherics from multiple sensors. GLD360 data has a 70% CG flash detection efficiency and a 5-10 km median CG stroke location accuracy [*Demetriades et al.,* 2010]. NLDN was used as ground truth for the validation of these detection efficiencies. The network reports peak current and polarity estimates but does not classify the strokes as CG or IC [*Said et al.,* 2010], however a classification of >|7 kA| and <|7 kA| for ICs and CGs respectively [*Holle,* 2009] were used for identification in this study.

2.2 3-Dimensional Lightning Networks

2.2.1 Oklahoma Lightning Mapping Array

The Lightning Mapping Array (LMA) was developed at the New Mexico Institute of Mining and Technology [*Krehbiel et al.,* 2000] and was modeled after the Lightning Detection and Ranging (LDAR) system developed for the Kennedy Space Center (KSC) [*Maier et al.,* 1995]. The LMA detects lightning flash by receiving radiation produced in a locally unused television channel (VHF channel 3) by a lightning channel segment as it propagates through space charge [*MacGorman et al.,* 2008]. The system is able to map total lightning activity, including IC and CG lightning, in all three spatial dimensions as a function of time.

In June of 1998 the LMA became operational in central Oklahoma. After a successful testing period the system was deployed in northwestern Kansas and Eastern Colorado as part of the Severe Thunderstorm Electrification and Precipitation Study (STEPS) in 2000. After STEPS 2000, the LMA was reinstalled in Oklahoma and consists of 11 stations approximately 15-20 km apart. Lightning can be mapped in three dimensions within 100 km of the center of the LMA system and plan location can be mapped within a 200 km range [*MacGorman et al.*, 2008].

2.2.2 Four-Dimensional Lightning Surveillance System

The Cape Canaveral Air Force Station (CCAFS) and NASA KSC is the busiest space launch center in the United States. In addition, CCAFS/KSC has the highest lightning frequency in the United States with a CG lightning flash density exceeding 9 flashes per km^2 per year [*Orville and Huffines*, 2001]. The LDAR [*Lennon and Maier*, 1991] system and the Cloud-to-Ground Lightning Surveillance System (CGLSS) [*Boyd et al.*, 2005] were the original two lightning sensing systems. The LDAR consists of 7 VHF antennas that sense impulsive emissions from lighting in the frequency range of approximately 60-66 MHz. The LDAR system detects IC lightning and produces a full 3-D spatial mapping of lightning discharge activity. The CGLSS system uses the same IMPACT sensors as the NLDN [*Biagi et al.*, 2007] to detect CG flashes [*Murphy et al.*, 2008].

The LDAR and CGLSS systems are limited in supportability and maintainability, so in 2008 these systems were upgraded and the network has been renamed the Four-Dimensional Lightning Surveillance System (4DLSS). The 4DLSS currently consists of 9 sensors, 7 of which are from the original LDAR network. With the two new sensors the spatial baseline extends about a factor of 2.5 wider than the original LDAR [*Murphy et al.*, 2008]. The lightning locations are

calculated with a new CP-8000 processor for both the CGLSS CG lightning and LDAR IC lightning [*Roeder*, 2010].

2.3 Analyzing Radar and Lightning Data

2.3.1 Tracking and Gridding

For each storm nearby NEXRAD Level II were obtained from the has.ncdc.noaa.gov website. For all scans ranging from 30 minutes before to 30 minutes after the jet, the latitude and longitude points of a polygon that surrounded the entire storm which produced the jet were identified using the Warning Decision Support System-II (WDSS-II) software. The average size of the cell that produced the jet was about 20 km x 20 km.

To grid the data two different methods were used. The first was using the NCAR SPRINT Radar Data Interpolation Software. This software interpolates radar measurements taken in spherical coordinate and coverts them to regularly-spaced latitude-longitude grids in height [*Mohr and Vaughn*, 1979].

For two of the cases there were errors in the radar data that were not resolved with SPRINT. Many algorithms can be written and used with the WDSS-II software which was developed by NSSL to manipulate radar data [*Lakshmanan et al.*, 2007; *Hondl*, 2003]. The w2merger algorithm takes in Level II WSR-88D data and can create mosaic data from multiple radars by transforming the data into latitude, longitude, height grids [*Lakshmanan et al.*, 2006]. For these two cases there was only one radar within range of the storms, but this algorithm can still be used to create grids for a single radar. An option of BeamSpread was chosen since it does not take into consideration the distance weighting options since there is only one radar to choose from. These gridded data resolved the errors by interpolating the data points that were available to the missing data points.

The output for both of these methods was a netcdf file with reflectivity data at each .01° in the horizontal and 1 km in the vertical. A script was written to convert this to a comma delimited file with time, latitude, longitude, height, and reflectivity value. From here, the reflectivity and lightning data within a polygon for each time period could easily be analyzed.

Satellite data was not able to be obtained for each case since most of the observations were during the night. Sounding data was taken from the closest site. The temperature and dewpoint vertical profiles were looked at as well as CAPE (convective available potential energy) and lifted index (LI) values. CAPE is the maximum energy available to an ascending parcel and can be represented by the following equation: $CAPE = \int_{p_n}^{p_f}(\propto_p - \propto_e)dp$ where p_f is the pressure at the level of free convection, p_n is the pressure at the level of neutral buoyancy, α_p is the specific volume of a parcel moving upward moist-adiabatically from the level of free convection, and α_e is the environmental specific volume. In a thermodynamic diagram, CAPE is the positive area between the lifted parcel process curve and the environmental sounding from the level of free convection to its level of neutral buoyancy. There are other ways to calculate CAPE as well such as surfaced based CAPE, most unstable CAPE, mean layer CAPE. These different CAPE calculations are computed based on temperatures from different pressure levels. For this study normal CAPE was used. Lifted Index can be defined as $L = T_L - T_{500}$ where T_L is the temperature of a parcel lifted from 850 mb to 500 mb and T_{500} is the temperature at 500 mb. LI is nominally identical to the Showalter index, except that the parcel being lifted (dry-adiabatically to saturation and then moist-adiabatically to 500 mb) is defined by the dry adiabat running through the predicted surface afternoon temperature maximum and the mean mixing ratio in the lowest 900 m of the sounding. A positive LI indicates a stable environment while a negative LI indicates an unstable environment. The more negative, the more unstable, increasing the

likelihood of severe thunderstorms if a lifting mechanism is present. [*Glossary of Meteorology*, 2000]

3. Gigantic Jet Cases

The GJs are summarized below by the geographic location in which they occurred. Two GJs occurred in Oklahoma, one in Florida, one in Puerto Rico, and two offshore near North Carolina. Each case is summarized by observations, environmental conditions, and discussion. These include where and when the jet occurred, the atmospheric soundings around the time of the jet, the formation of the storm, and radar and electric structure via cross sections, contoured frequency altitude diagrams, and time series plots.

3.1 Oklahoma

3.1.1 Observations

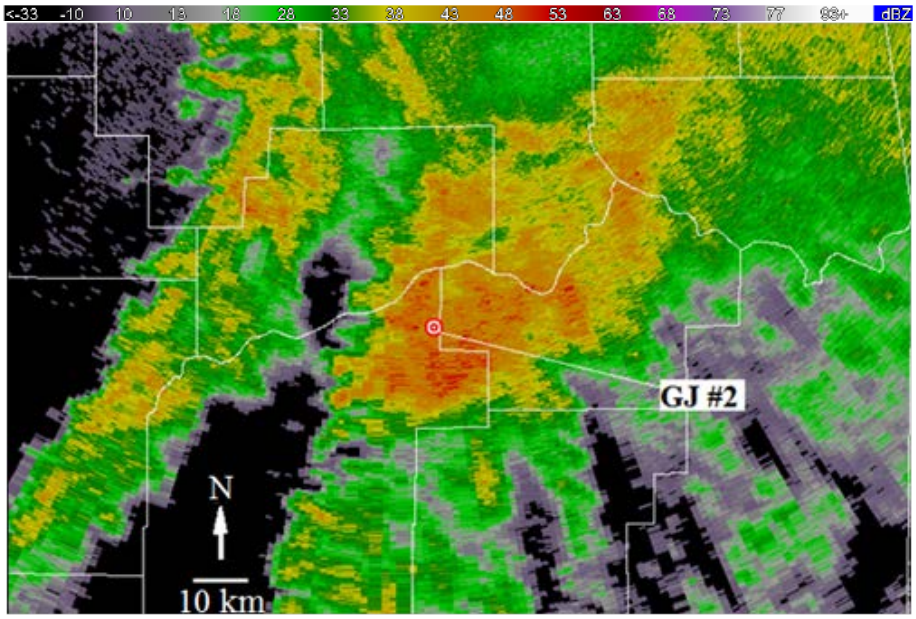

Figure 3. Plan view of the KINX radar at 728:38 UTC, the location of the second jet is marked. The counties are outlined in white and the background is black.

Two negative GJs were recorded in eastern Oklahoma on 9 September 2010 at 7:22 UTC and 7:28 UTC, respectively. The GJs were observed from Hawley, Texas (32.66°N, 99.84°W) from a Watec 902H2 camera stamped with exact GPS time ~500 km away from the storm [*Lu et* al., 2011b]. A negative sprite was also observed at 6:49 UTC in this storm. The GJs were within 225 km of the Oklahoma LMA [*MacGorman et* al., 2008]. This is a little far for accurate 3D mapping

but the upper lightning structure can still be resolved. 2D NLDN data was also available for this storm. Figure 3 shows the base, .5° tilt, reflectivity data from the KINX radar at the time of the second GJ (7:28 UTC). The warmer the colors, the more intense the precipitation is. This storm contained a significant warm rain process with the low CAPE and LI, but very moist vertical profile.

3.1.2 Environment

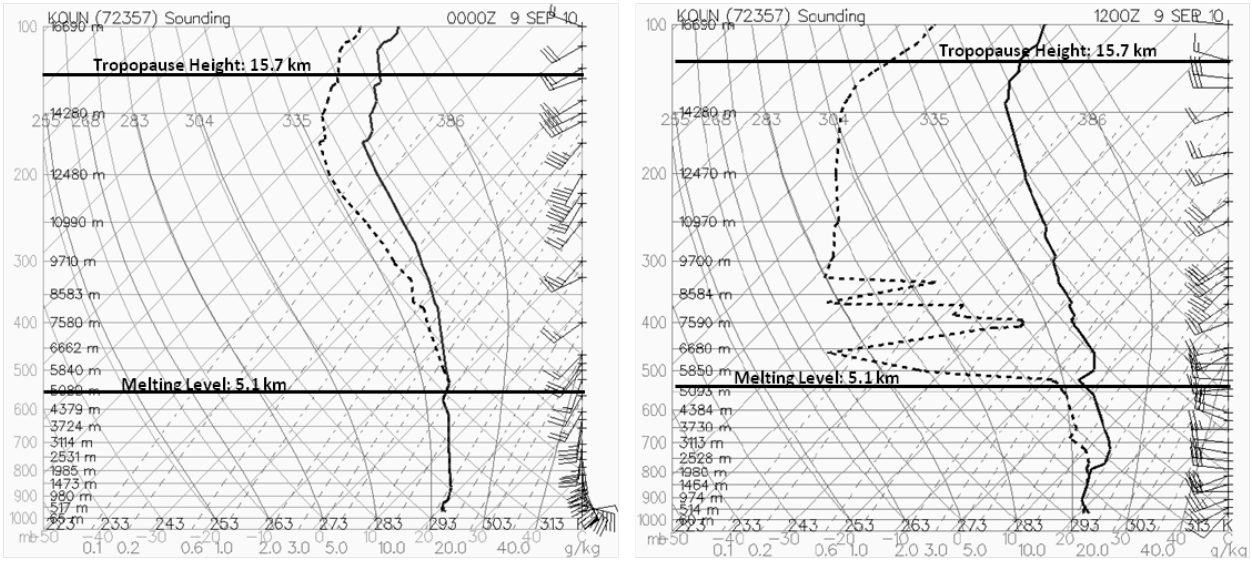

Figure 4. Sounding data from Norman, OK at 00 UTC (a) and 12 UTC (b). The vertical dashed line is the dewpoint and solid line is temperature. The solid black horizontal lines are the melting level and tropopause heights.

The storm producing the two negative jets was a strong thunderstorm embedded in the remnants of tropical storm Hermine. Hermine developed off the coast of southeastern Mexico 5 days prior to the jet observations. Many tornado, wind, and flooding reports were recorded throughout Texas and Oklahoma as Hermine made its way inland. Hermine was still considered a tropical depression when the GJ-producing storm formed. The environment was very moist and tropical-like. Two soundings from Norman, Oklahoma (KOUN) at 0 UTC and 12 UTC were examined since the time of the jets were in the middle of both (Figure 4). The 0 UTC sounding showed the temperature profile was completely saturated below 6 km indicating it was likely raining, which was verified by radar. By 12 UTC the system had moved to the northwest and the

upper levels, predominately above the melting level, had dried out. The first 2 km were still fairly moist. Both soundings had very similar melting and tropopause heights of 5.1 km and 15.7 km respectively. The CAPE values were 45 J/kg and 18 J/kg, both of which are extremely low, indicative of a tropical-like airmass. More shear and a lower LI, .27, was found in the 0 UTC sounding, but significant thunderstorm conditions were not present.

3.1.3 Discussion

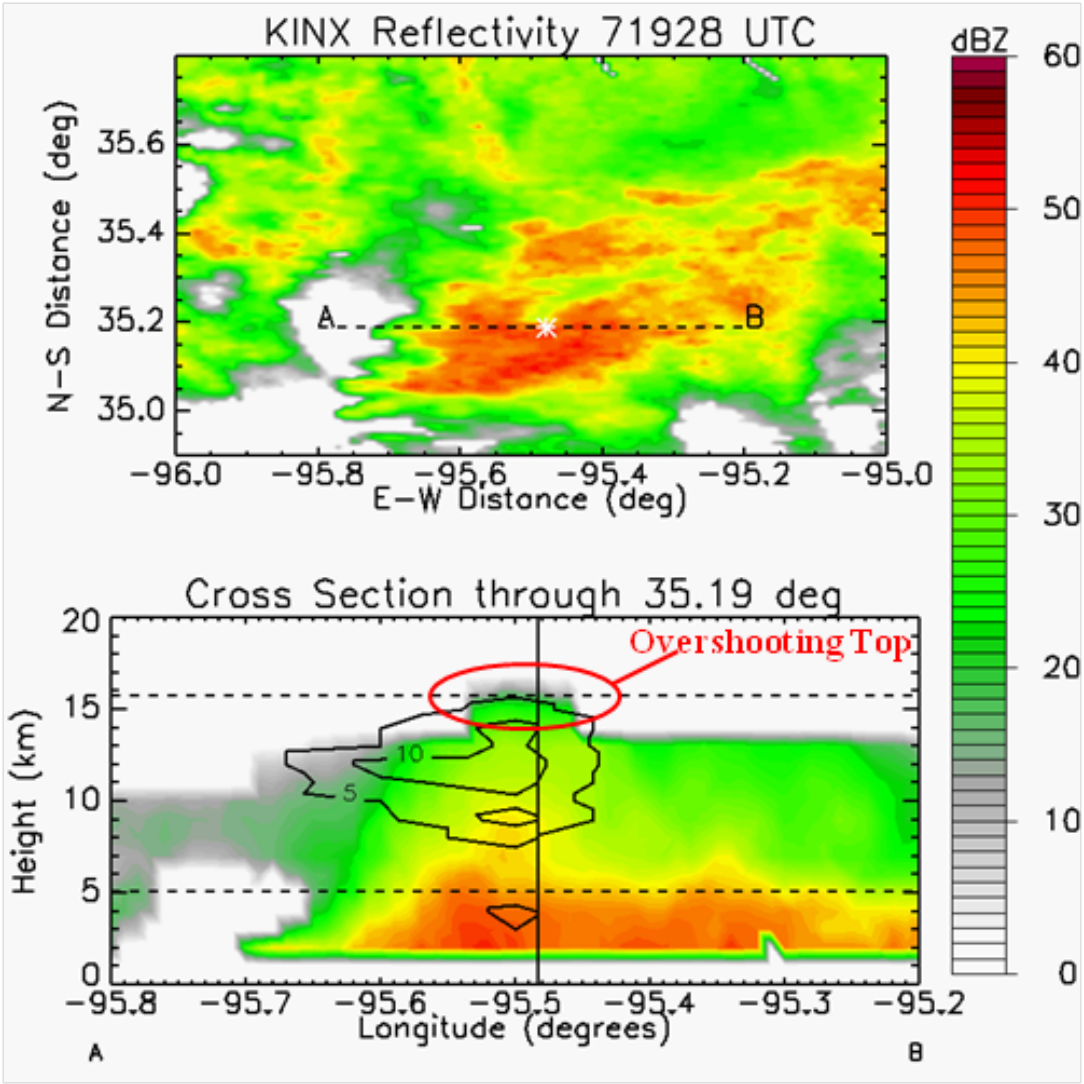

Figure 5. Plan view of KINX radar reflectivity data at the time of the first GJ. The dotted line represents the area of the vertical cross section. The GJ is marked by white * (top). The cross section with the melting level and tropopause height (horizontal lines), jet location (vertical line), and overshooting top labeled (bottom). Contoured in black are the OK-LMA lightning sources.

A vertical cross section through the area of the first GJ was produced. Also overlaid are the LMA lightning source data contoured in one-km bins (Figure 5). A lightning source maximum was located around the area of the first GJ. The bulge in reflectivity at the storm top was identified as an overshooting top punching through the local tropopause. The maximum reflectivity in this storm was 54-dBZ at 2 km, 8 minutes before the first jet formed. The 10-dBZ echo top was ~15.5 km above mean sea level, indicating tall storms do form in low CAPE environments, like the tropics

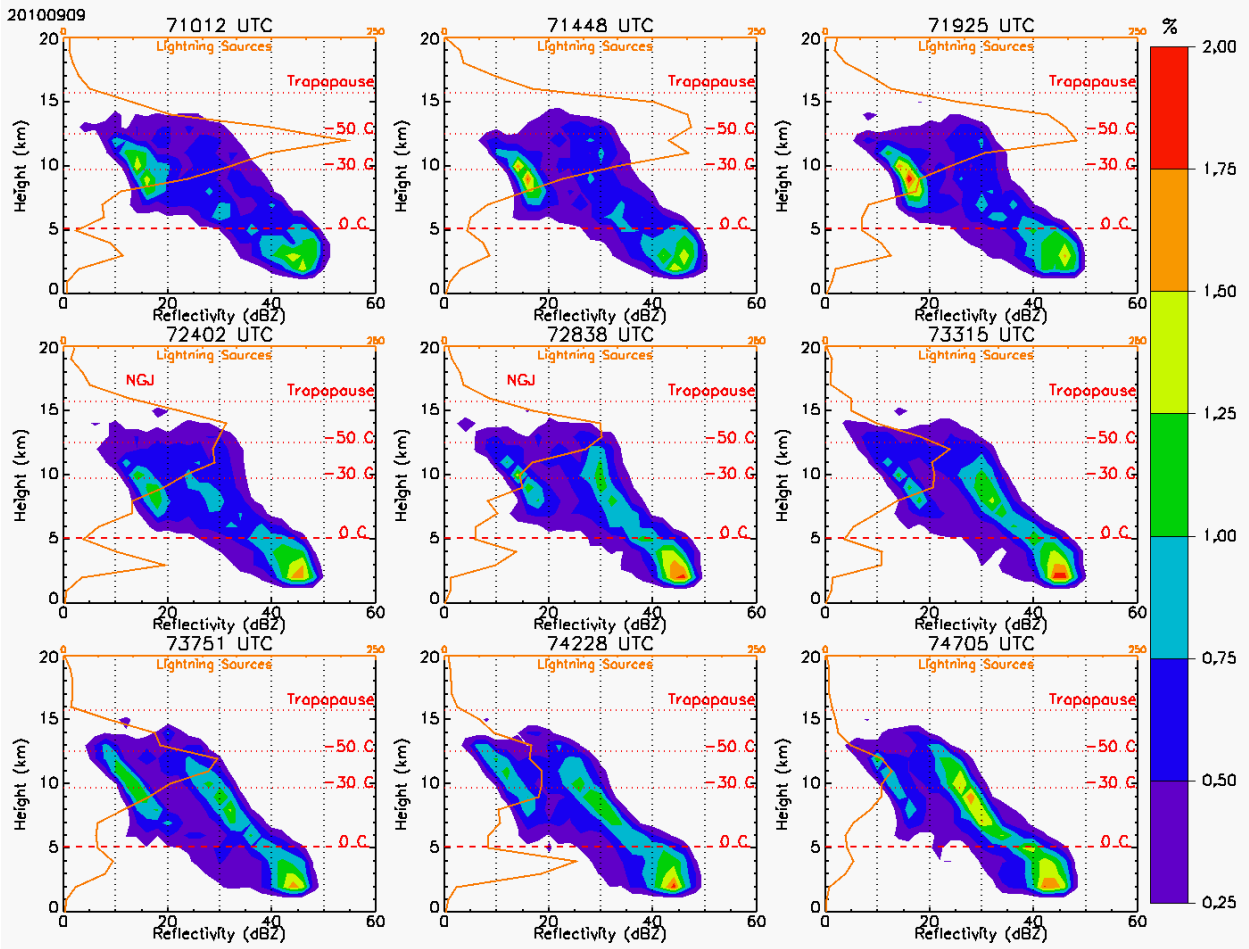

Figure 6. Contoured frequency by altitude diagram (CFAD) show the normalized distribution of reflectivity in 5 minute bins versus height for four time steps around the time of the jets. "GJ" is labeled in the diagrams when the jet occurred. The lightning source frequency is plotted over one km levels in orange. Isotherms are plotted in red dashed lines.

Contoured frequency by altitude diagrams (CFADs) [*Yuter and Houze*, 1995] for the Oklahoma storm were constructed and overlaid with LMA lightning data (Figure 6). Both lightning source density and height of the peak lightning source increased leading up to the first GJ. The lightning source density peak was just below the -50° C isotherm. Here, the sources are a small burst of VHF radiation associated with lightning or local electrical breakdown; however -50° C is too cold for supercooled water so this brings into question any role of non-inductive charging. The frequency of sub-35-dBZ values increased with height, creating a bulge above 10 km and a 2% frequency maximum in ~15 dBZ at the time of the first jet. This increase in upper level reflectivity frequency suggested a strong updraft lofting ice particles indicating the storm is at an intense stage. After the first jet, the storm weakened which was indicated by a decrease in lightning sources and the frequency of reflectivity at mid-levels. The frequency in low level, high reflectivity increases at this point as well, indicating the large, precipitation sized particles are falling out from the storm. According to *Krehbiel et al.* [2002], intensification in upper-level lightning, an increase in the height of the LMA source density peak, and overshooting radar echo tops indicate a convective surge.

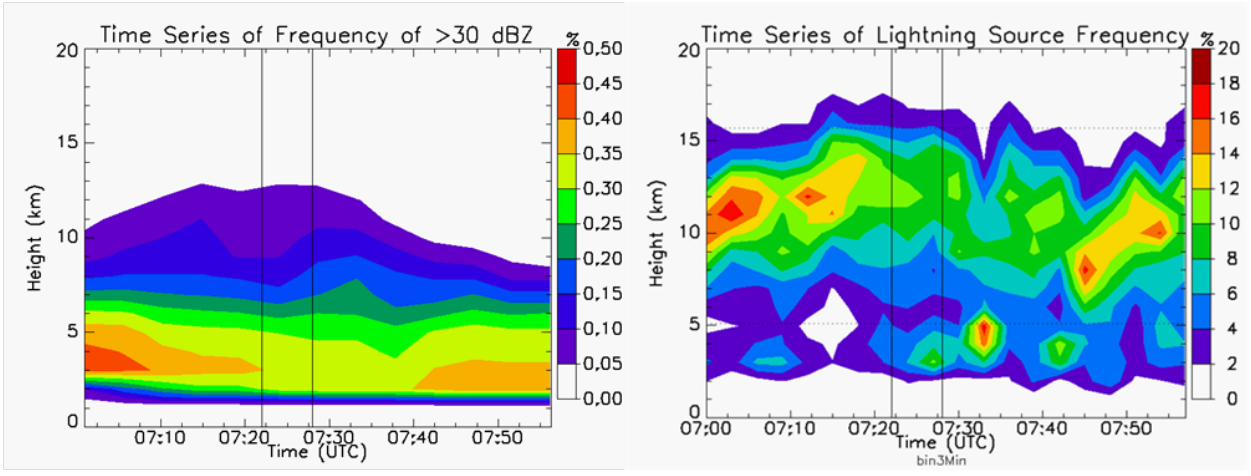

Figure 7. Time series plots of the frequency of >30 dBZ versus height in one km levels with the jet time denoted by the black vertical line (left). Time series of the normalized three-dimensional source frequency versus height (right). The vertical black lines are the time of the jets.

Time series plots of lightning and reflectivity frequency also show the presence of a convective surge. Figure 7a showed a peak of >30-dBZ frequency just before the first jet, flattened out until the second jet, and then dropped off. A time series of the VHF source density from the LMA showed quite a few oscillating peaks. However, the two peaks a few minutes before the first jet are the only peaks reaching above 17 km (Figure 7b). After the jets occurred there was a dip in the lightning source density in the upper levels. The jets occurred just after the storms peak intensity.

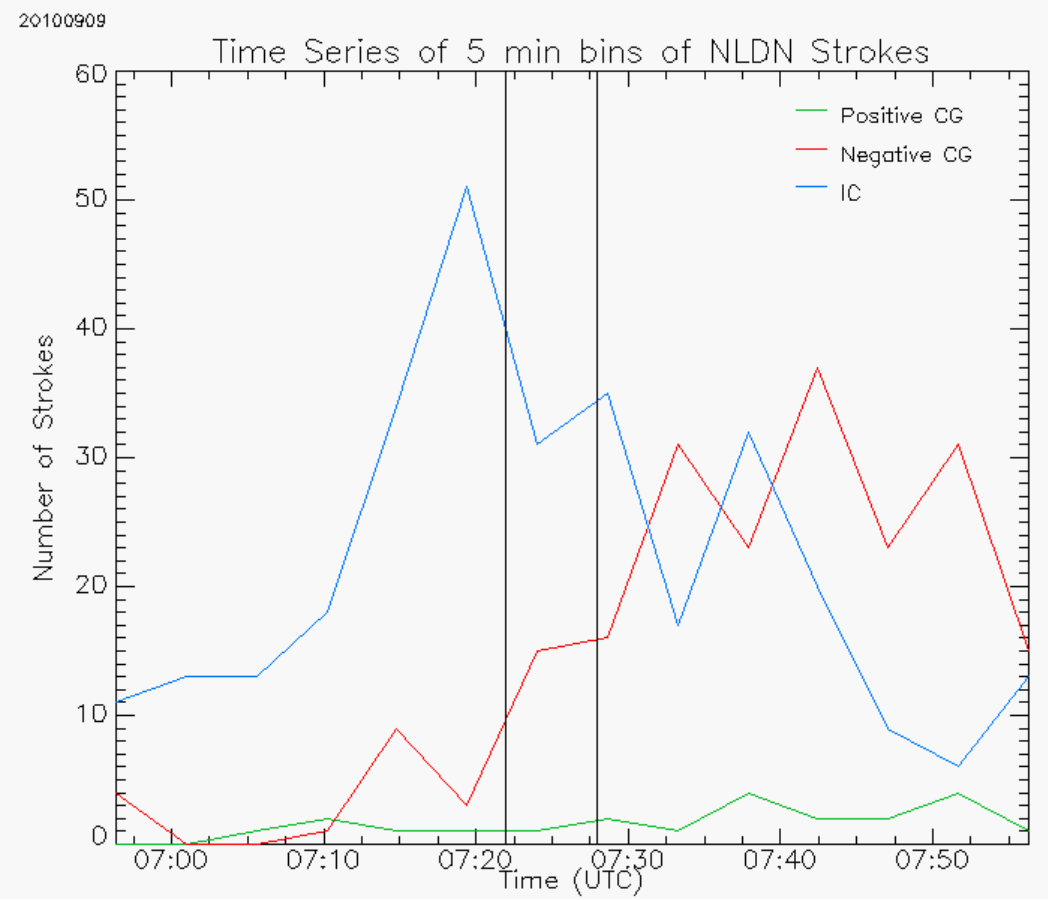

Figure 8. A time series plot of NLDN for lightning strokes in five minute bins versus height (one km levels). Positive CGs (green), negative CGs (red), IC (blue) are plotted with the time of the GJs (---).

The 2-dimensional NLDN lightning data time series plot shows the storm was predominately producing negative CG lightning (Figure 8). Very little CG lightning was present the 20 minutes

before the first GJ, suggesting a buildup of an overall net negative charge. The IC lightning peaked just before the first GJ and the negative CG lightning picked up after the second jet, again indicating the storm was still intensifying during the GJ time period

A relatively high-topped storm formed in tropical depression Hermine producing two gigantic jets within 6 minutes of each other. The overshooting top and peak in upper level lightning as well as the reflectivity characteristics indicated the storm had just reached its peak intensity when the GJs were produced.

3.2 Florida

3.2.1 Observations

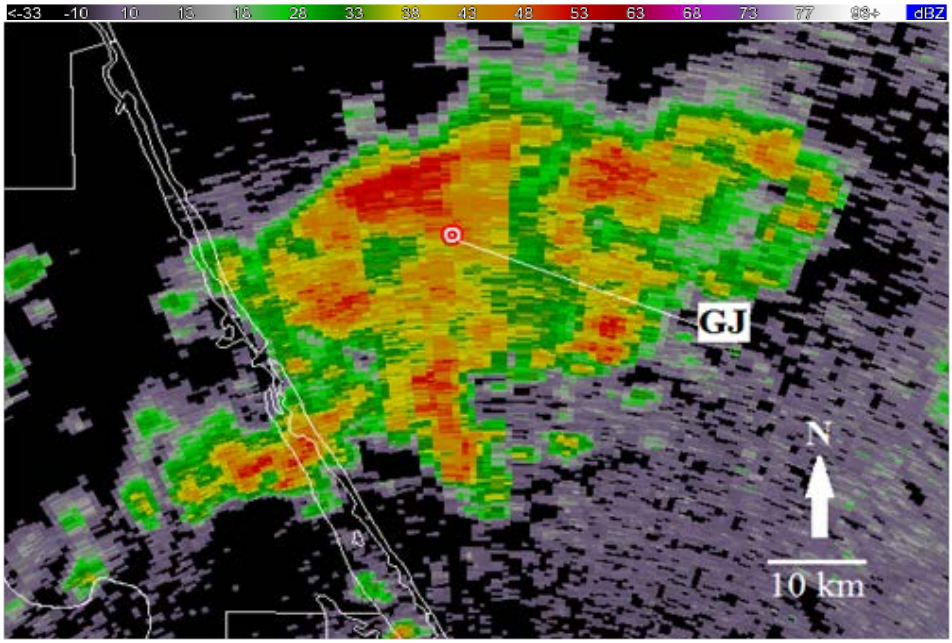

Figure 9. Plan view of reflectivity from the KMLB radar at 11:00:46 UTC, the location of the jet is marked.

On 28 September 2010, another negative GJ was recorded in Sebring, Florida (27.52°N, 81.52°W). A Watec 902H2 camera was used to capture the jet, the same type used in the Oklahoma case. The GJ occurred off the east coast of Florida at 11:01 UTC ~70 km north of the 4DLSS [*Roeder*, 2010]. Figure 9 shows the plan view of the Florida storm with the best

estimated jet location. This storm was also well within detection range of the NLDN [*Cummins and Murphy*, 2009].

3.2.2 Environment

The jet-producing storm formed within a cluster of other storms but it had the highest reflectivity values of others in the area and stayed intense the longest, however it was never able to become isolated. The sounding was taken from Tampa (KTWB) at 12 UTC, an hour after the jet occurred (Figure 10). The melting level was similar to the Oklahoma case at 4.9 km with a dry slot above the melting level. However, the tropopause was about one km higher at 16.7 km and the CAPE values were ~2500 J/kg with a LI of -4.8. These parameters are much more indicative of severe thunderstorms compared to tropical, warm-rain processes.

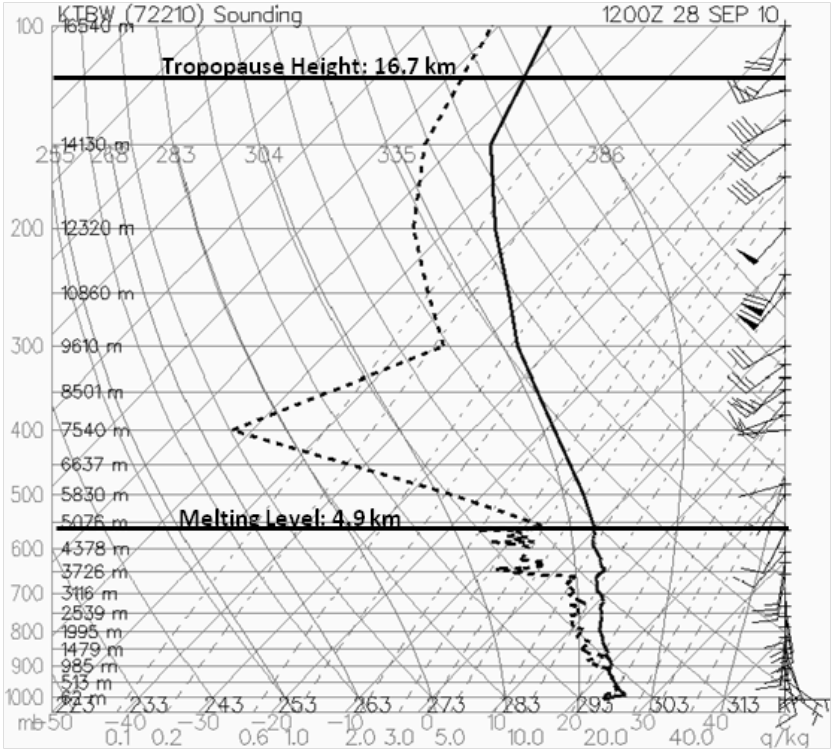

Figure 10. Sounding data from Tampa at 12 UTC. The vertical dashed line is the dewpoint and solid line is temperature. The solid black horizontal lines are the melting level and tropopause heights.

3.2.3 Discussion

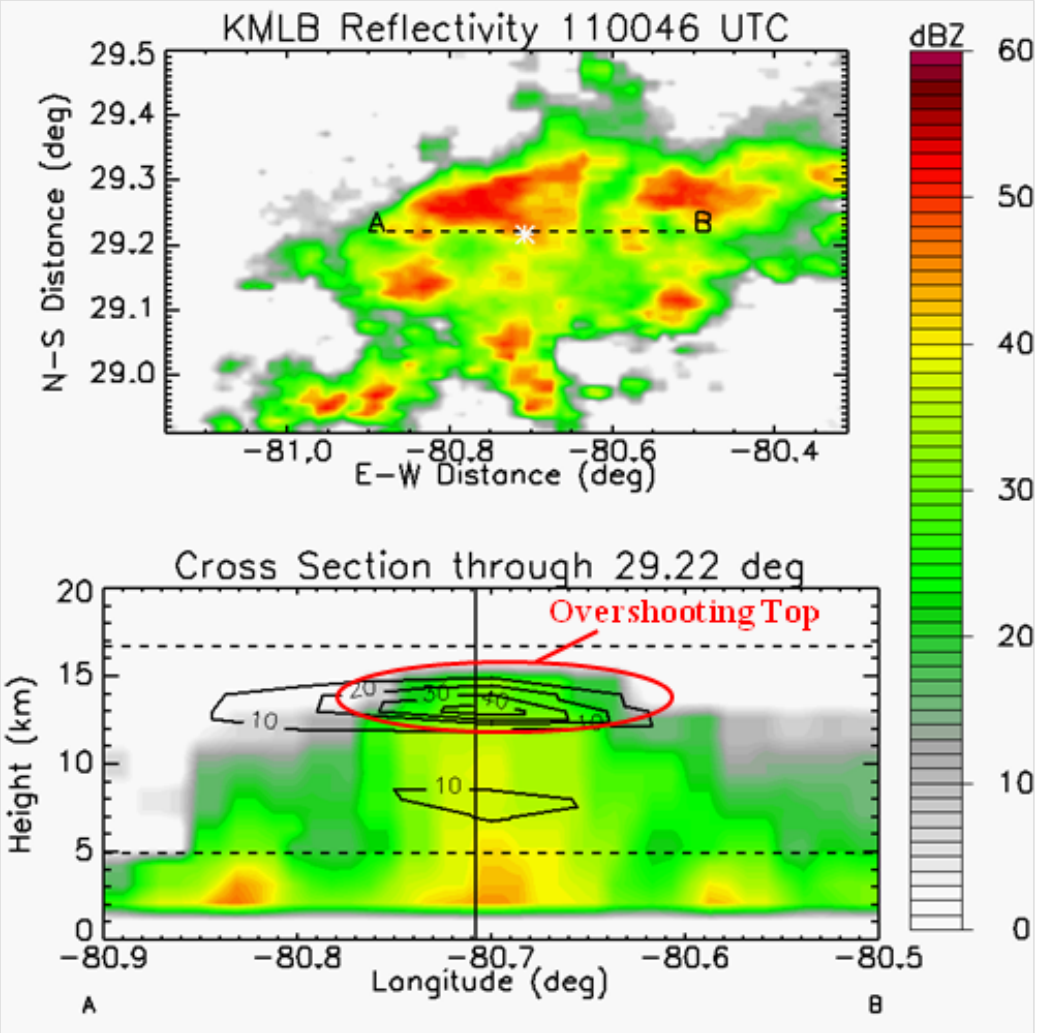

Figure 11. Plan view of KMLB radar reflectivity data at the time of the GJ. The dotted line represents the area of the vertical cross section. The GJ is marked by white * (top). The cross section with the melting level and tropopause height (horizontal lines), jet location (vertical line), and overshooting top labeled (bottom). Contoured in black are the 4DLSS lightning sources.

A plan view of reflectivity data at the surface and a vertical cross section with 4DLSS sources is shown in Figure 11. The storm structure was very similar to the Oklahoma case; the lightning maximum is concentrated in an overshooting top region, however the overshooting top in this case did not punch through the tropopause. This storm reached a peak reflectivity of 59 dBZ 20 minutes before the GJ. The maximum reflectivity was quite a bit higher than the Oklahoma case, which then can be attributed to a more severe thunderstorm verses a tropical-like

thunderstorm as in the Oklahoma case. At the time of the jet there was a maximum reflectivity of 53-dBZ and 10-dBZ echo tops at 14.2 km.

The CFAD for the Florida case had very similar results with an intensification of the storm leading up to the jet and a weakening of the storm after the jet (Figure 12). Reflectivity values of 35-dBZ reached 14 km just before the time of the jet. The peak lightning sources were around the -50° C isotherm with the strongest peak at 13 km five minutes after the GJ. Like in the Oklahoma case, this brings into question any role of non-inductive charging. In the frames leading up to the jet the higher frequency values are above 5 km indicating the storm was strengthening. No lightning was detected in the last two frames.

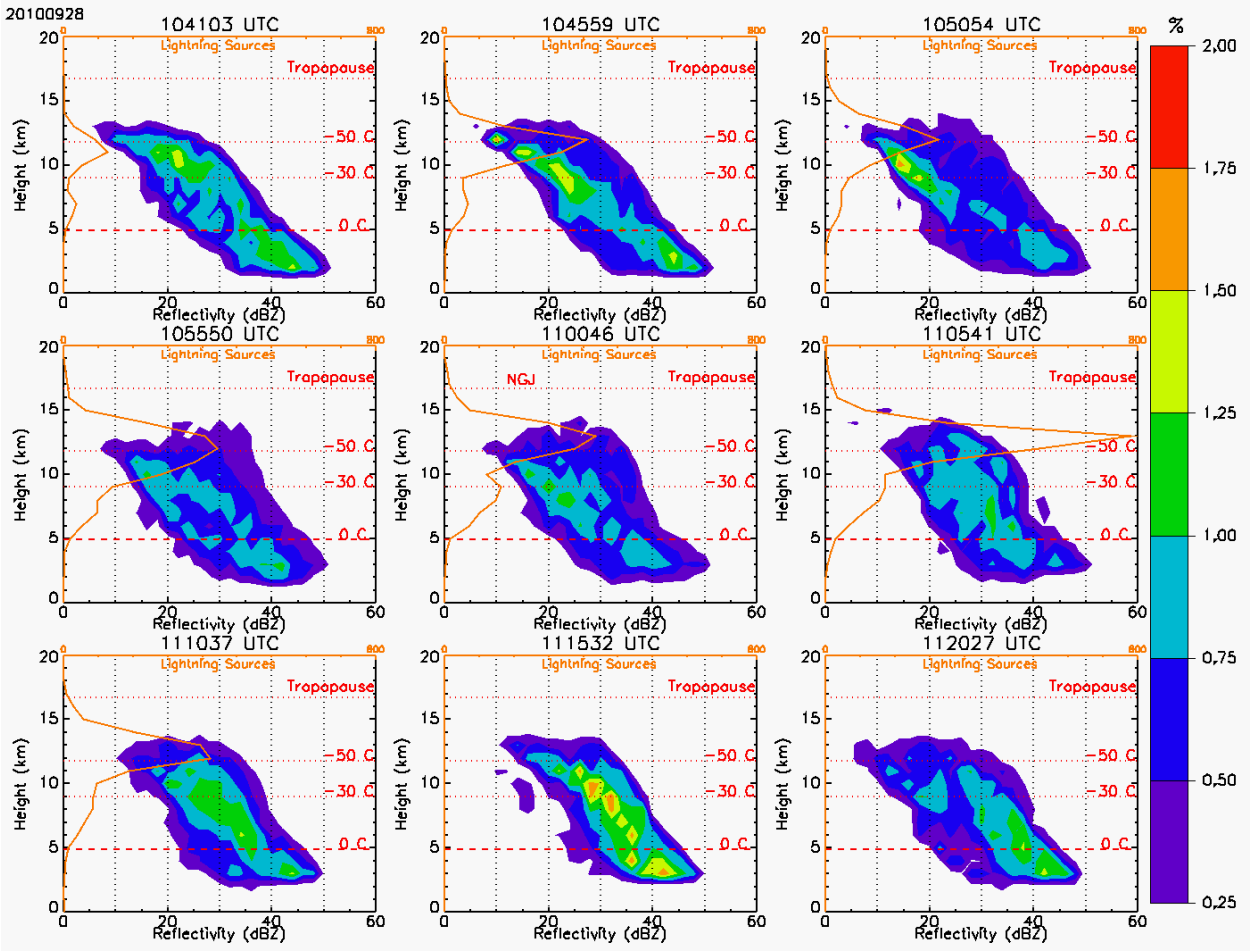

Figure 12. CFAD plots show the normalized distribution of reflectivity in 5 minute bins versus height for four time steps around the time of the jets. “GJ” is labeled in the diagrams when the jet occurred. The lightning source frequency is plotted over one km levels in orange. Isotherms are plotted in red dashed lines.

A time series plot for reflectivity values over 30 dBZ was produced for 30 minutes before and after the jet (Figure 13). Again, this plot shows what the CFADs did with a peak reflectivity just before the time of the jet in the upper levels. At the 0-4 km region there is a minimum in frequency around the time of the jet. This can be explained by a strong updraft lifting the particles upwards. A lightning frequency time series plot was produced as well using the 4DLSS data (Figure 13). A clear lightning maximum at 15 km was present at the time of the jet lasting about 5 minutes. At this time there was also a minimum of lightning in the 7-11 km region. Lightning intensity in the mid-levels picked up after the jet.

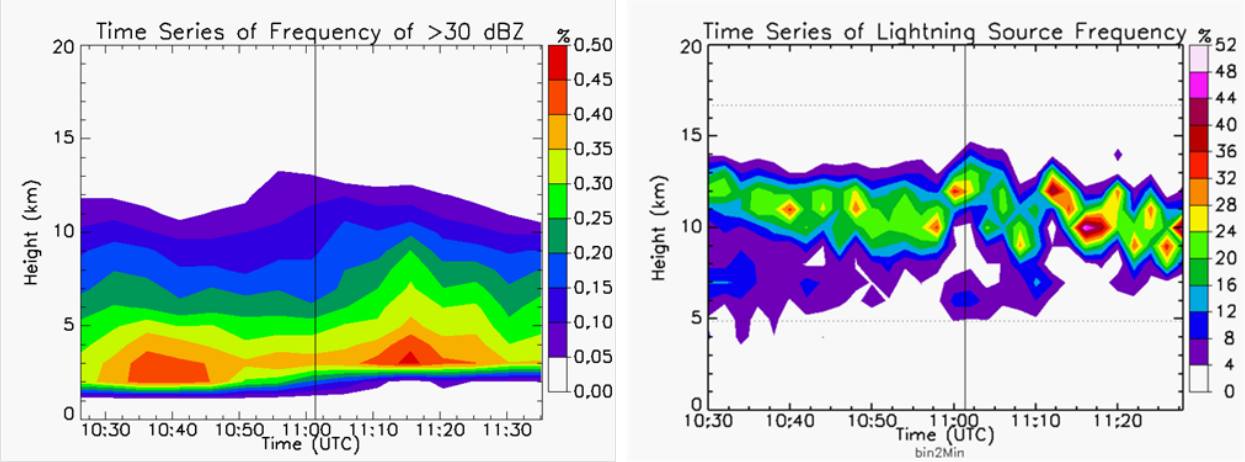

Figure 13. Time series plots of the frequency of >30 dBZ versus height in one km levels with the jet time denoted by the black vertical line (left). Time series of the normalized three-dimensional source frequency versus height (right). The vertical black lines are the time of the jets.

The NLDN data was plotted as a function of time as well to distinguish the type of lightning that was occurring (Figure 14). The storm was IC dominant but still had more negative CG's than positive CGs. Like the Oklahoma case, this storm had little to no CGs leading up to the jet and an increase in negative CG after the GJ. The absence of CG lightning leading up to the storm suggests the storm was intensifying.

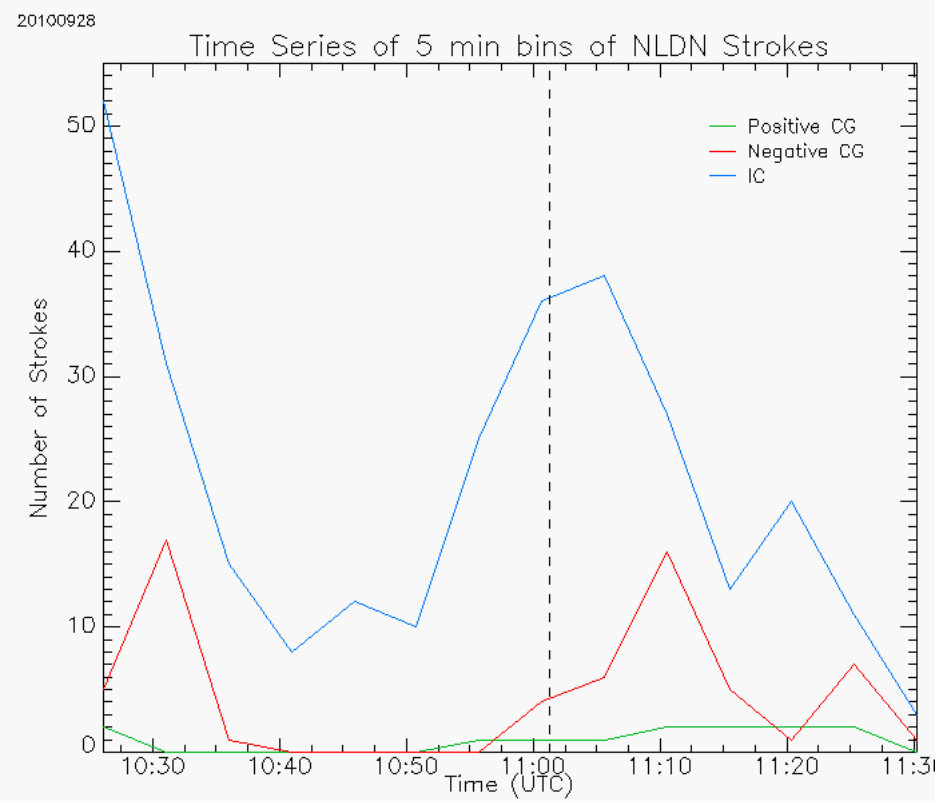

Figure 14. A time series plot of NLDN for lightning strokes in five minute bins versus height (one km levels). Positive CGs (green), negative CGs (red), IC (blue) are plotted with the time of the GJs (---).

The environment the Florida storm formed in was more of a thunderstorm environment compared to the tropical environment of the Oklahoma case, however both storms had very similar features. The maximum height of reflectivity occurred about 5 minutes before the jet and the peak lightning frequency occurred in the 5 minutes after the jet. NLDN data showed the storm was negative CG dominant with the majority lightning being IC. A lull in CG lightning leading up to the jet suggested storm intensification.

3.3 Puerto Rico

3.3.1 Observations

On 22 September 2011 another negative GJ was recorded with a Kodak Z749 digital camera on a tripod with a time stamp of 5:27 UTC from eastern Puerto Rico (18.05°N, 67.11°W). The jet was in the middle of the island along a 68° azimuth from the camera location,

but the exact location of the GJ could not be pinpointed. In Figure 15 the camera location was labeled with the 68° azimuth drawn intersecting two possible cells for the Puerto Rico case. Analysis was performed for the area in the red box, which included both cells since that were only ~5 km apart. Puerto Rico is outside the NLDN range, thus the GLD360 was analyzed.

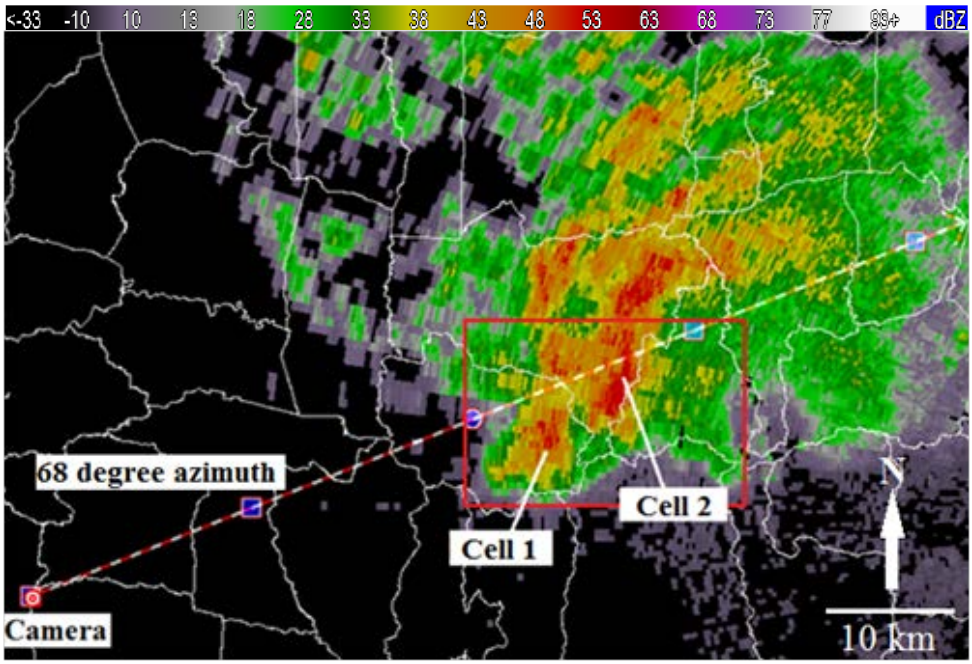

Figure 15. Plan view of the TJUA radar at 05:28:29 UTC, the two possible cells are marked along with the camera location and azimuth. The red box is the area radar analysis was performed.

3.3.2 Environment

The two storms in the vicinity of the jet were the strongest cell in the area, like the previous cases. All the convection was embedded with no isolated storms. The sounding was taken from Puerto Rico (TJUA) at 0 UTC, about 5.5 hours before the jet (Figure 16). The melting level was the same as the previous cases at 5 km and the tropopause height was a little bit lower and 14.6 km. The atmosphere was fairly moist but did not have a significant dry layer like the other cases. The CAPE values were ~ 3500 J/kg with a LI of -5.95, indicative of a good environment for thunderstorms to form in.

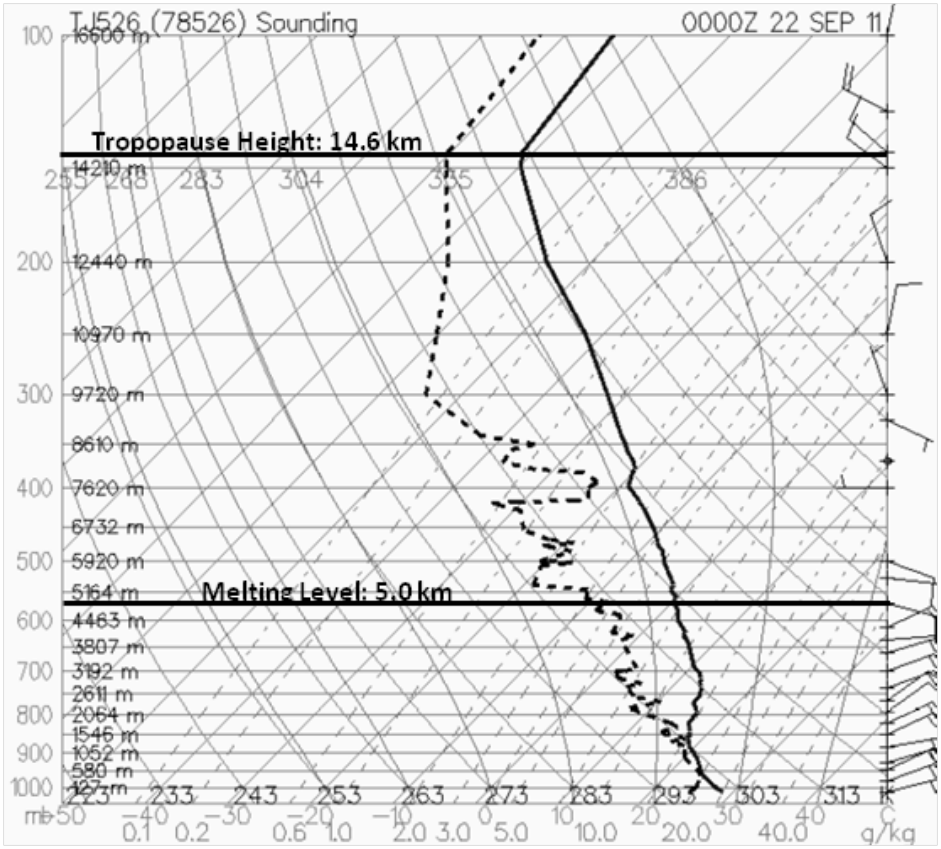

Figure 16. Sounding data from Puerto Rico at 0 UTC. The vertical dashed line is the dewpoint and solid line is temperature. The solid black horizontal lines are the melting level and tropopause heights.

3.3.3 Discussion

As stated before, the specific cell that produced the Puerto Rico jet could not be uniquely identified and 3D lightning mapping observations were not available for analysis; however, the storm structure can still be analyzed with radar observations. For the Puerto Rico case a cross section was drawn through both possible cells (Figure 17) and the cell closer to the camera had a small overshooting top similar to the other cases. The storm further from the camera did not have an overshooting top. The maximum reflectivity was 57-dBZ 5 minutes prior to the jet, with an echo top height of 15 km, again similar to the Oklahoma and Florida cases.

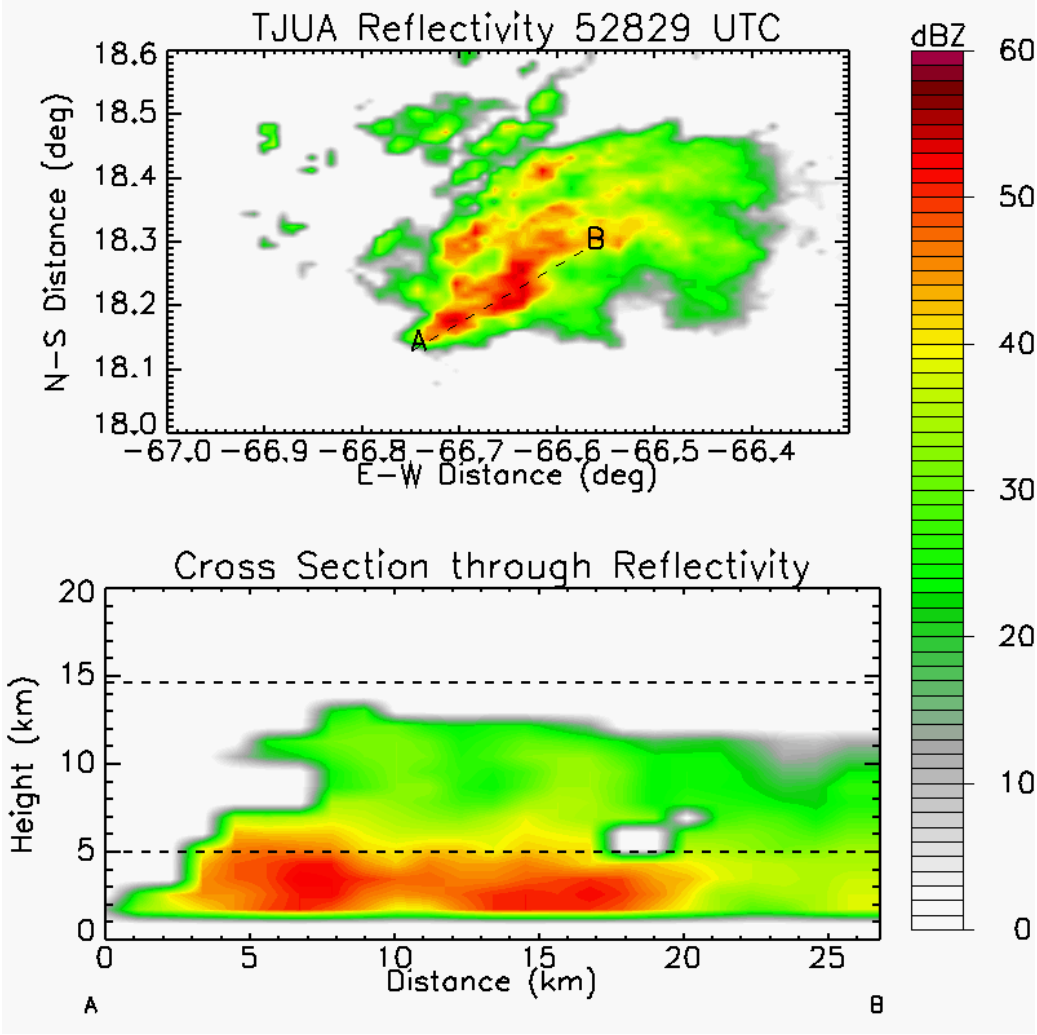

Figure 17. Plan view of TJUA radar reflectivity data at the time of the GJ. The dotted line represents the area of the vertical cross section. The GJ is marked by white * (top). The cross section with the melting level and tropopause height (horizontal lines) (bottom).

Like the previous cases, CFADs were produced however only reflectivity frequency was plotted since there were no 3D lightning data. Reflectivity data for both possible storms was included in the analysis since they were less than 5 km apart. A bulge in 20-30 dBZ pushed through the tropopause height leading up to the time of the jet. The 5 minutes after the jet occurred was the peak frequency of 25-dBZ in the upper levels indicating the storm was at its peak intensity. The next few scans showed the bulge in the upper reflectivity values start to

decrease and the frequency of the 30-dBZ increase near the lower levels suggesting the heavy precipitation was raining out (Figure 18).

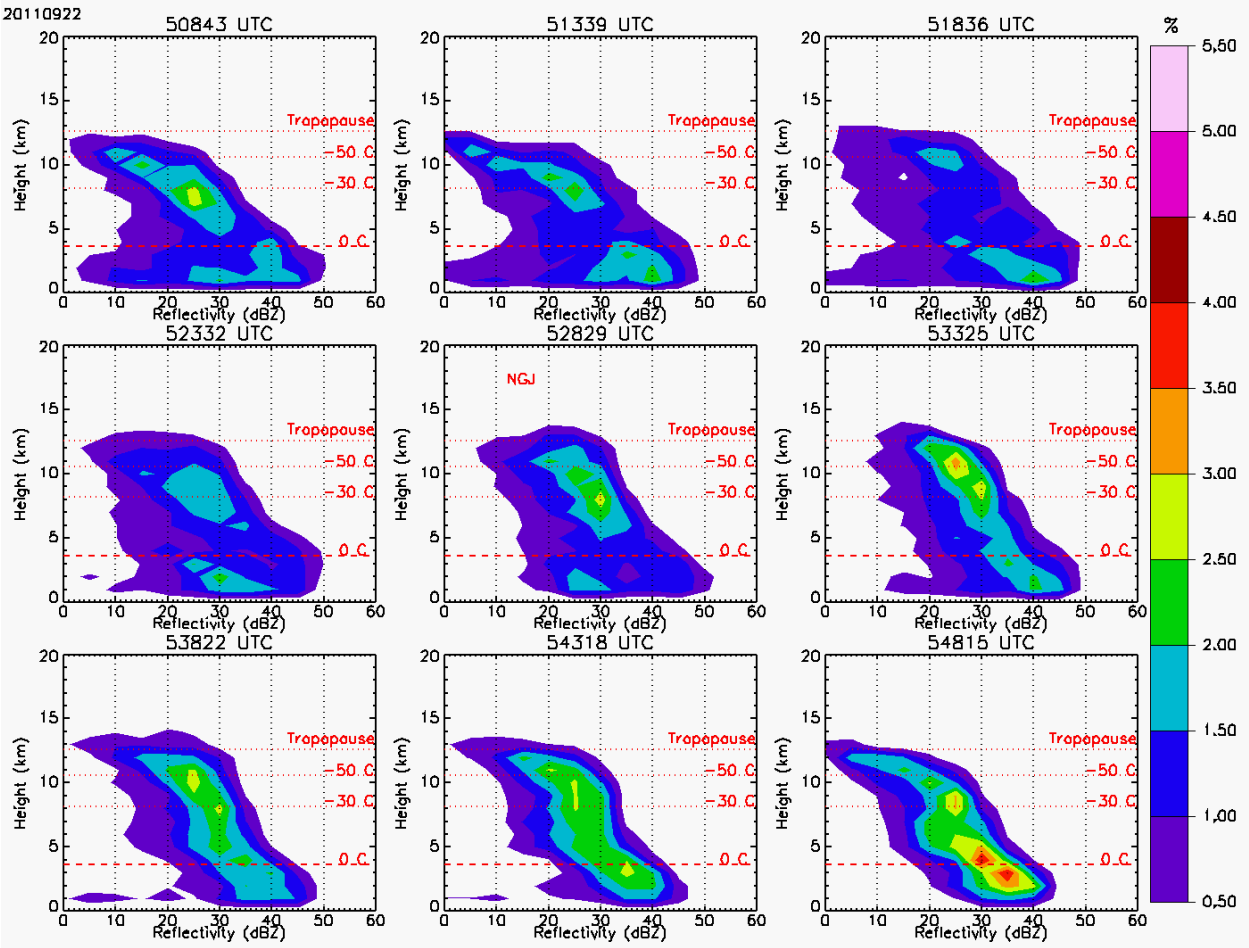

Figure 18. CFAD plots show the normalized distribution of reflectivity in 5 minute bins versus height for four time steps around the time of the jets. “GJ” is labeled in the diagrams when the jet occurred.

The time series reflectivity plot showed similar results to the CFAD. A peak height of >30-dBZ frequencies occurred just a minute after the time of the jet. Similar to the Oklahoma and Florida case there was a minimum frequency of >30-dBZ in the lower layers suggesting the particles were being lofted by a strong updraft at the time (Figure 19).

As stated above, GLD360 stroke data was used for the Puerto Rico case. Figure 20 shows a limited number of strokes detected. This is due to a lower CG flash detection efficiency and greater location accuracy uncertainty than NLDN [*Demetriades et al.*, 2010]. Overall the storm

was negative CG dominant with a large peak density 5 minutes before the jet occurred. The lull in CG lightning was not as apparent in this case since the total number of flashes were so limited. The Puerto Rico case was fairly similar to the previous cases.

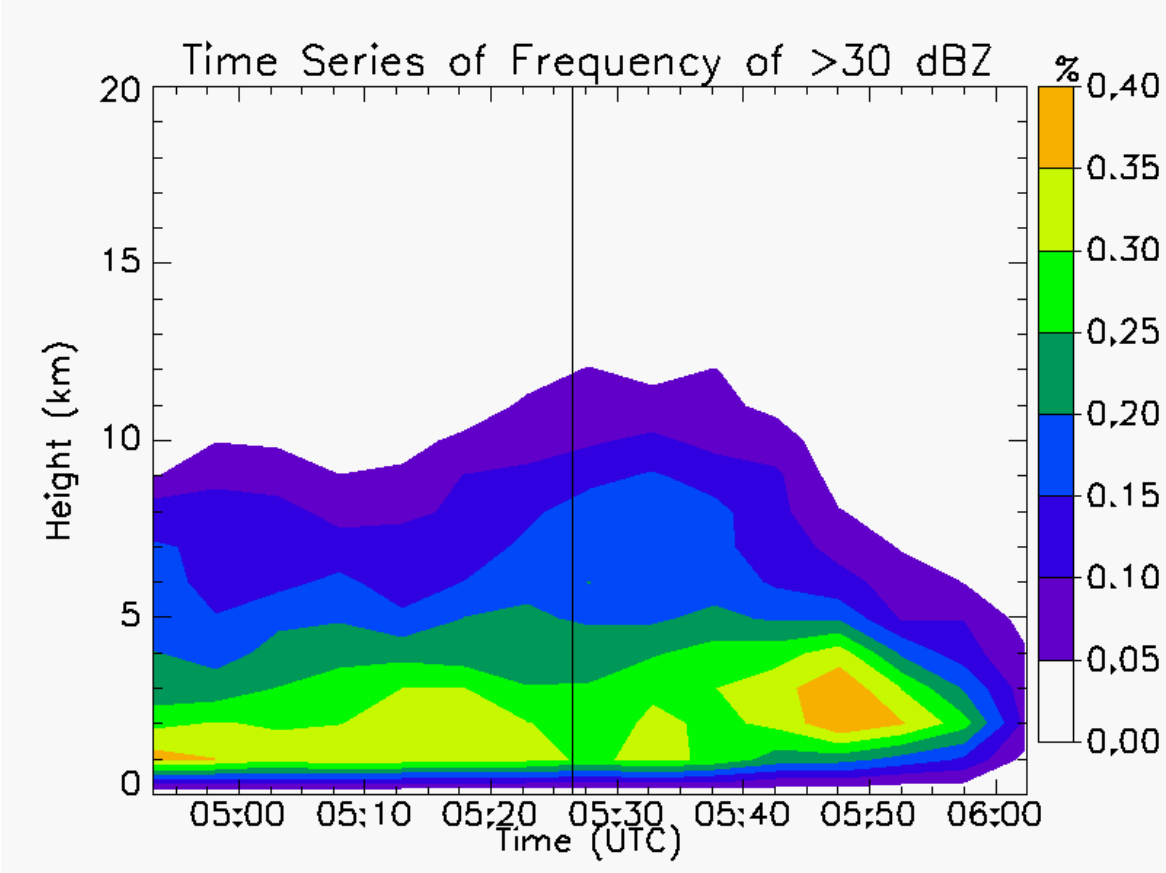

Figure 19. Time series plot of the frequency of >30 dBZ versus height in one km levels with the jet time denoted by the black vertical line for 20110922.

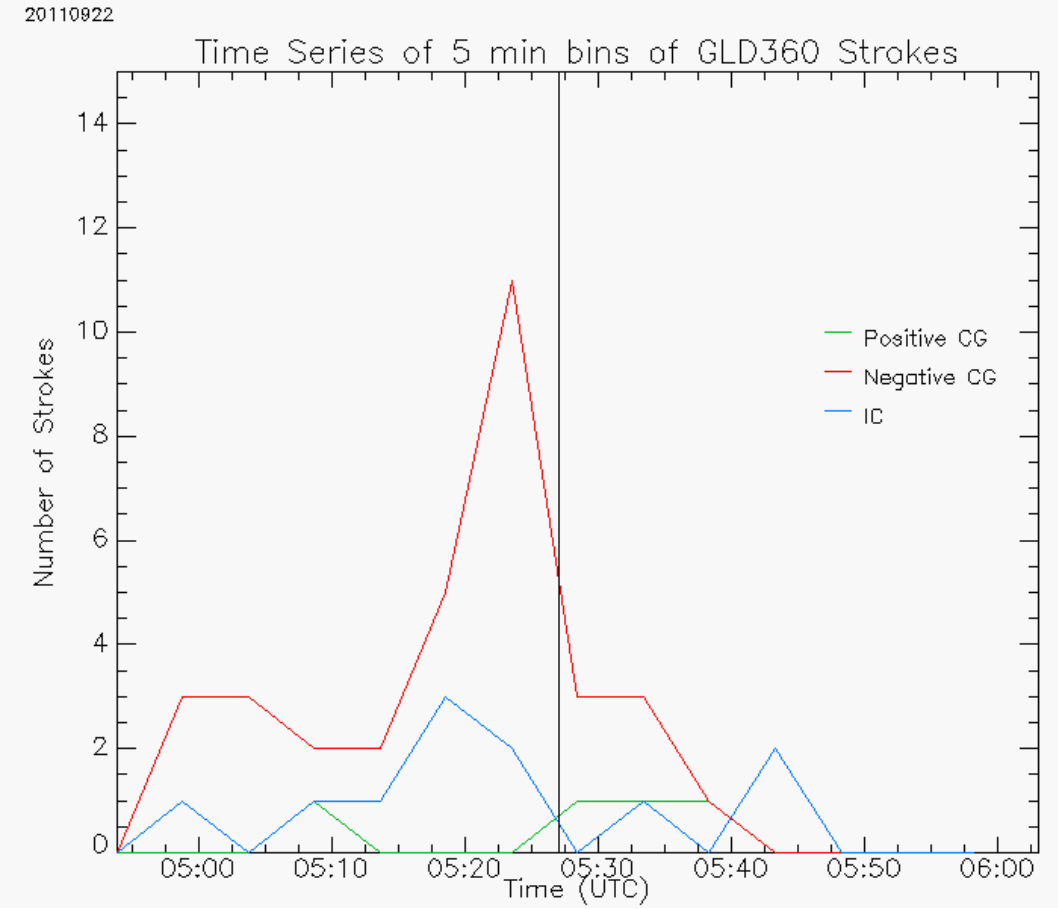

Figure 20. A time series plot of NLDN for lightning strokes in five minute bins versus height (one km levels). Positive CGs (green), negative CGs (red), IC (blue) are plotted with the time of the GJs (---).

3.4 North Carolina

3.4.1 Observations

Two GJs have been recorded off of the coast of North Carolina since 2009, one being negative and another being positive. The negative jet was recorded on 8 May 2009 at 8:08 UTC. The positive jet was observed on 17 April 2011 at 3:11 UTC. Both of these GJs were recorded from a WATEC 902H2 ultimate low light charge device camera coupled to a triggered video acquisition system that records approximately one second of video when specified trigger criteria are met. This camera is located in a field near Duke University (35.975°N, 79.100°W) [*Cummer et al.*, 2009]. The exact point of the negative GJ could not be pinpointed, but it was seen along a 117°-118° azimuth. Figure 21a shows the plan view reflectivity with the azimuth range shaded.

The exact location of the jet cannot be pinpointed, however it was apparent which cell produced the jet. The positive GJ occurred at 34.23°N, 76.21°W, in a squall line off of the coast of North Carolina (Figure 21b) [*Lu et al.*, 2011a]. Like the Puerto Rico case there were no LMA's in the area, however both of these GJs were within NLDN range. The KMHX radar in Morehead, North Carolina was used to analyze the reflectivity data.

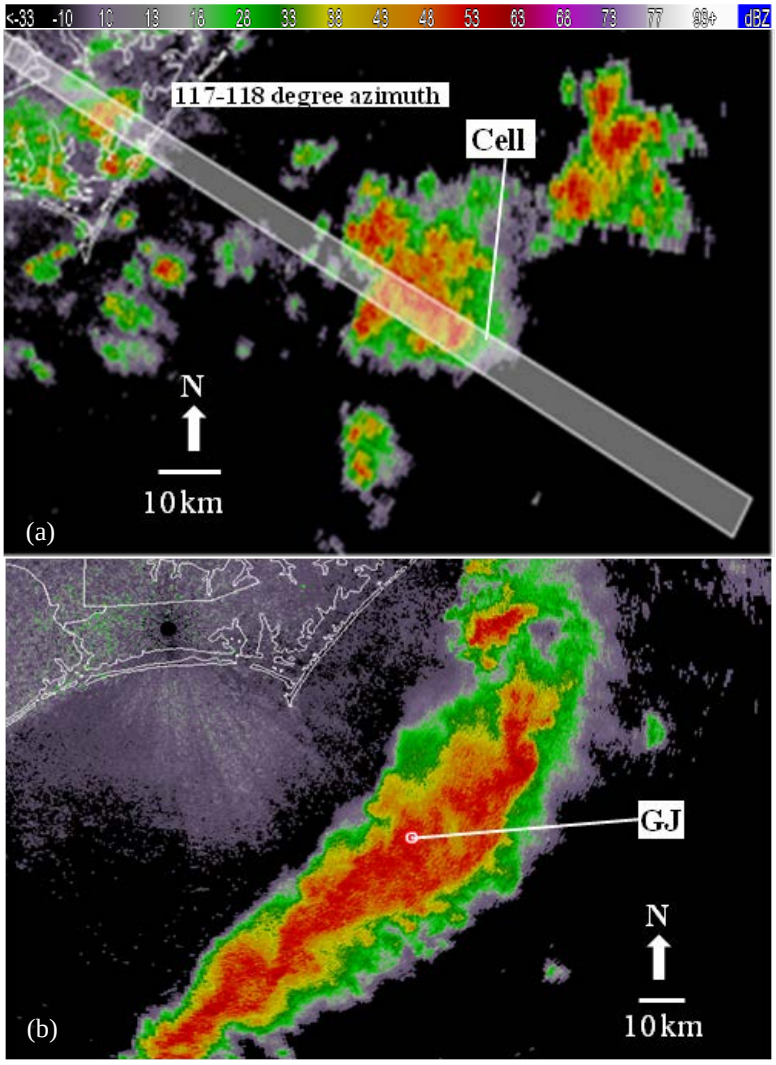

Figure 21. (a) Plan view of the KMHX radar at 08:06:27 UTC, azimuth is shaded; the cell that produced the GJ is labeled. (b)Plan view of the KMHX radar at 03:09:15 UTC. The jet location is labeled.

3.4.2 Environment

The storm that the negative GJ initiated from was an isolated storm, the largest in the area with a few other fairly isolated cells in the area. The positive jet however occurred in the

northern edge of a squall line moving off the coast. The soundings for both North Carolina cases were taken from Morehead City, North Carolina. The 2009 negative GJ sounding at 0 UTC shows a similar feature to the Oklahoma and Florida cases with a very dry layer above the melting level. The melting level and tropopause heights were a few kilometers lower though, at 3.6 km and 12.5 km respectively (Figure 22a). The CAPE values were ~1200 J/kg and LI of -2.8. Similarly, the 2011 positive GJ case sounding at 0 UTC had a melting level and tropopause height of 3.8 km and 12.9 km respectively (Figure 22b). The sounding for the positive jet had a dry layer similar to the other cases, but it was below the melting level. CAPE values were 2300 J/kg and LI of -6.4. Both of the soundings suggested a good environment for thunderstorm formation.

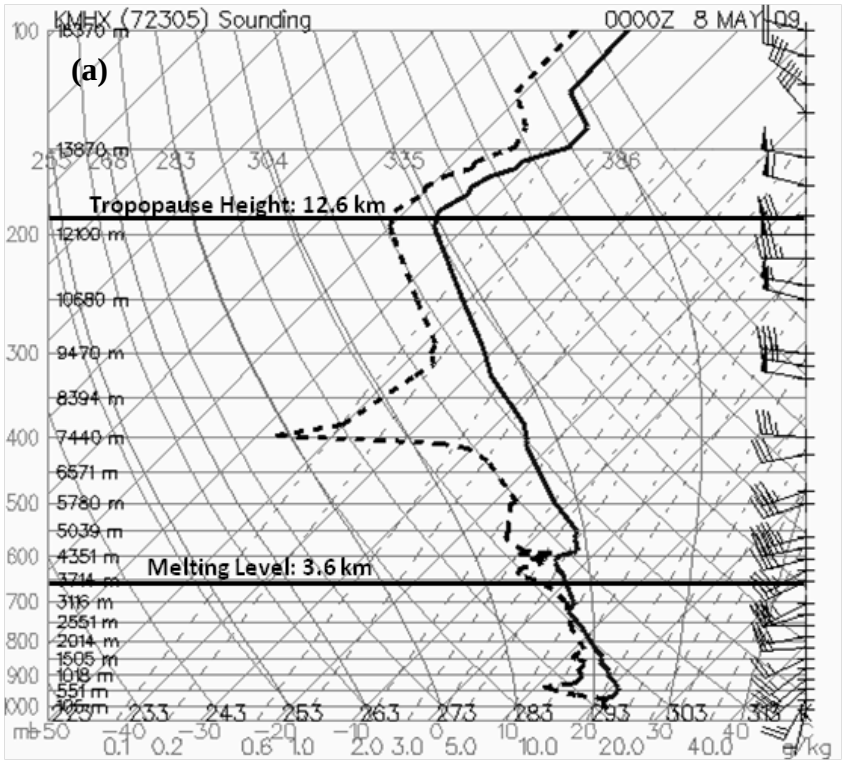

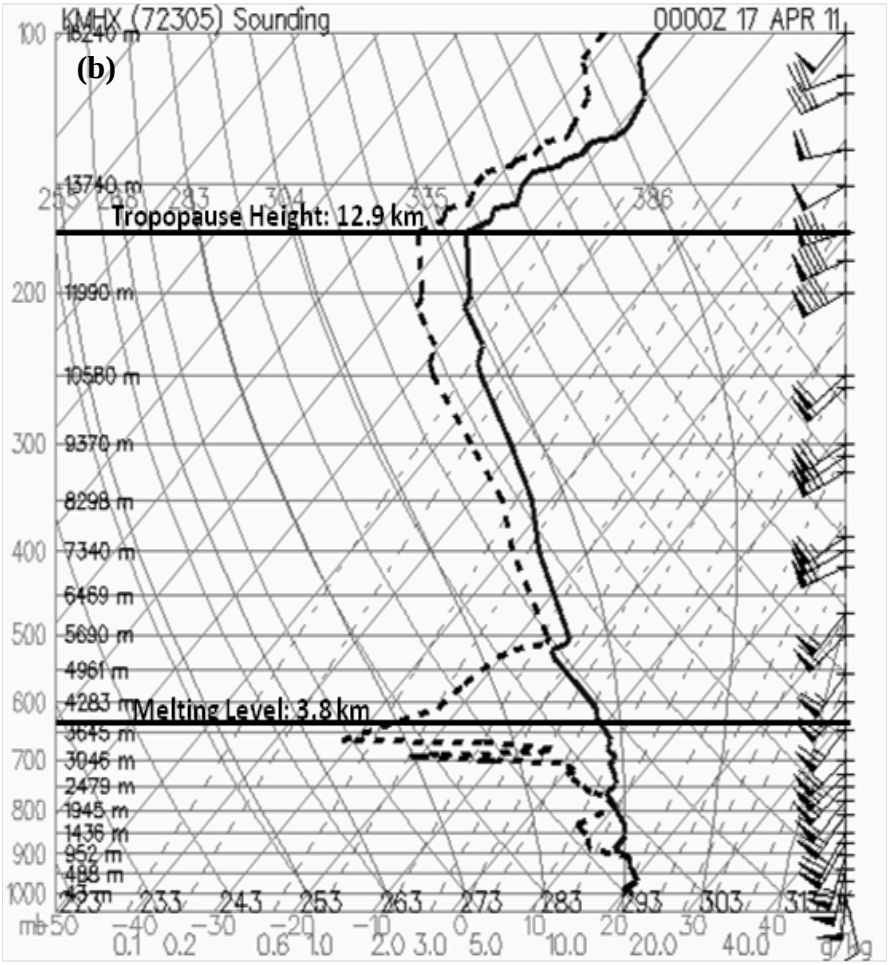

Figure 22. Sounding data from Morehead, NC at 0 UTC on (a) 20090508 and (b) 20110417. The vertical dashed line is the dewpoint and solid line is temperature. The solid black horizontal lines are the melting level and tropopause heights.

3.4.3 Discussion

A cross section of the 2009 negative GJ North Carolina case is shown in Figure 23. Again, the exact location of the jet is unknown but initiated from this isolated cell. The cell was about 110 km away from the KMHX radar. The cross section does not show an overshooting top for this case. There is a short wide area of elevated reflectivity maximum, but is questionable to be called an overshooting top. The maximum reflectivity in this storm was 62-dBZ about 15 minutes before the jet. The 10-dBZ echo top height was about 14 km msl, the lowest of all the cases examined in this thesis. The 2011 positive GJ North Carolina case is shown in Figure 24. The squall line was about 90 km from the KMHX radar and the location of the jet is noted with

the white star in the plan view and the vertical line in the cross section. This storm also did not have a clear overshooting top however there is a small region of 15-20 dBZ above the tropopause. This storm had a peak reflectivity value of 62 dBZ with 10-dBZ echo tops at 16 km msl. Since there are no LMA networks in North Carolina we cannot address the relationships to VHF source density for these two cases.

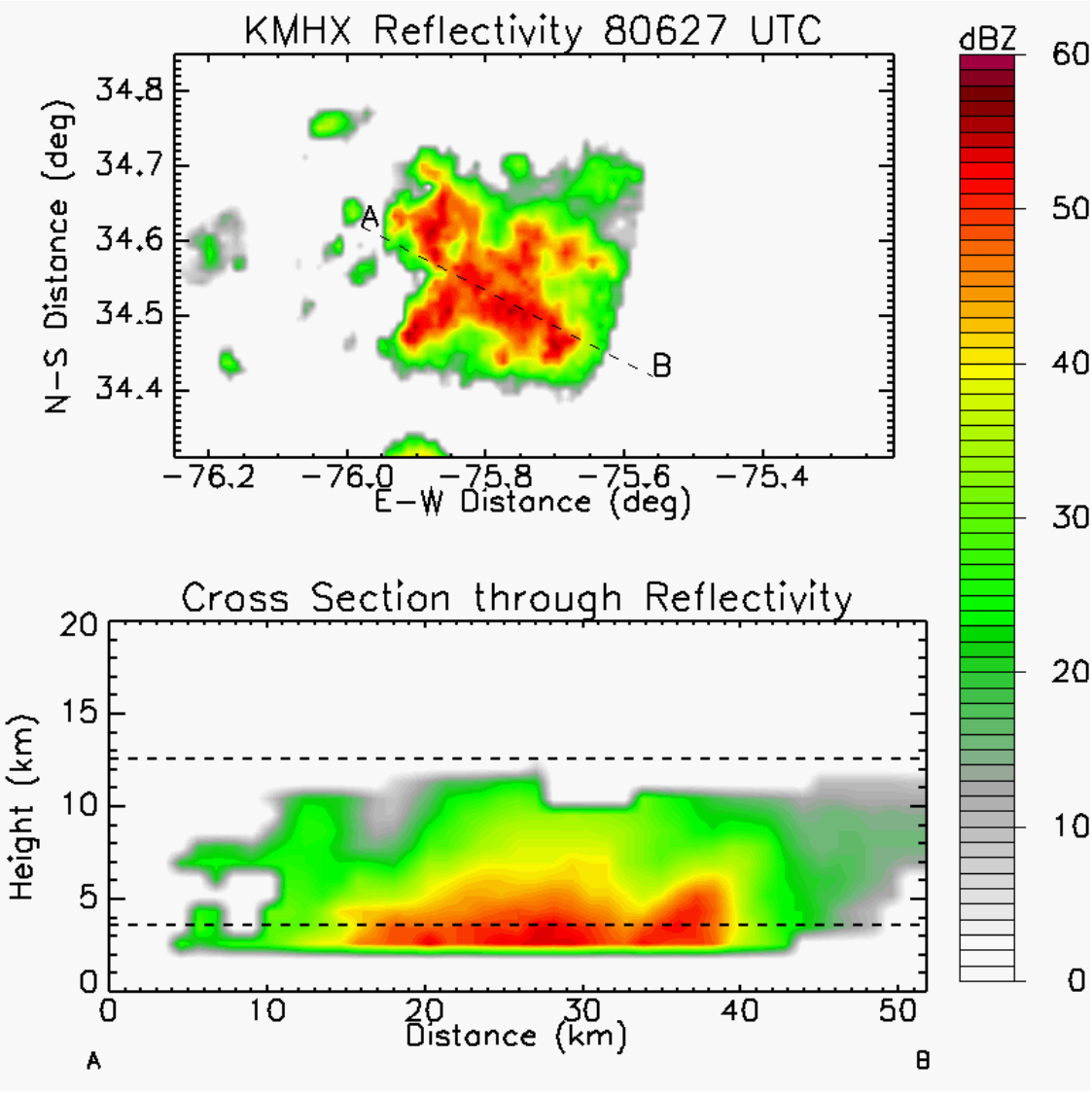

Figure 23. Plan view of KMHX radar reflectivity data at the time of the GJ. The dotted line represents the area of the vertical cross section. The GJ is marked by white * (top). The cross section with the melting level and tropopause height (horizontal lines) (bottom).

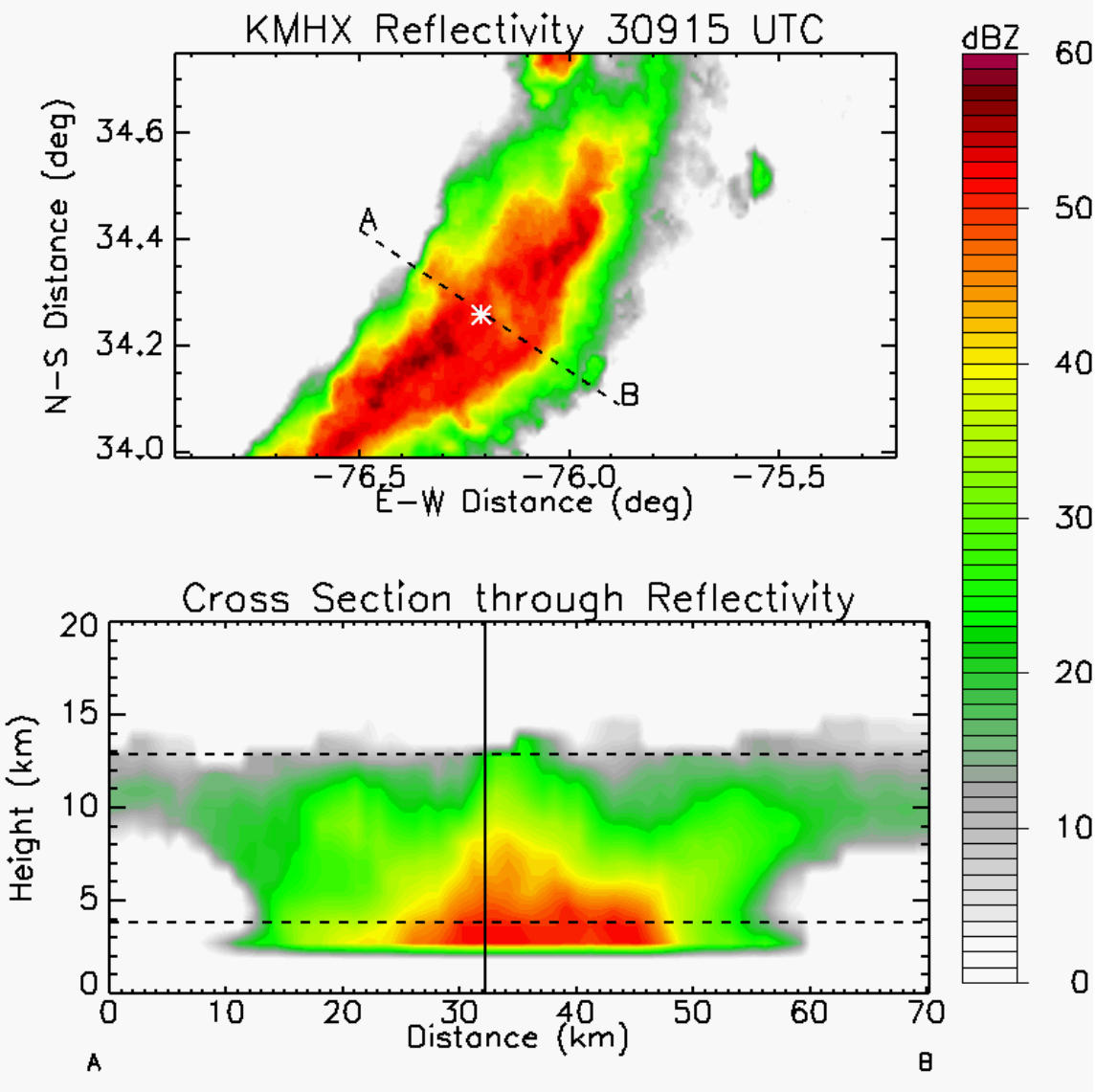

Figure 24. Plan view of KMHX radar reflectivity data at the time of the GJ. The dotted line represents the area of the vertical cross section. The GJ is marked by white * (top). The cross section with the melting level and tropopause height (horizontal lines) and jet location (vertical line) (bottom).

The CFAD plots for the negative jet showed different results compared to the previous cases. There was a small bulge of 35-dBZ present between the -30° C and -50° C isotherms in the first frame, but decreases leading up to the time of the jet suggesting the storm was weakening. However the frequency of 10-20 dBZ values in the upper levels continued to increase throughout the whole time period, possibly suggesting a strong updraft lofting particles (Figure 25). The positive jet case was closer to the previous cases. A bulge of 30-40 dBZ became more prevalent

leading up to the time of the jet. By the last frame the maximum frequency was in the lower 5 km indicating this was when the storm was raining out and weakening (Figure 26).

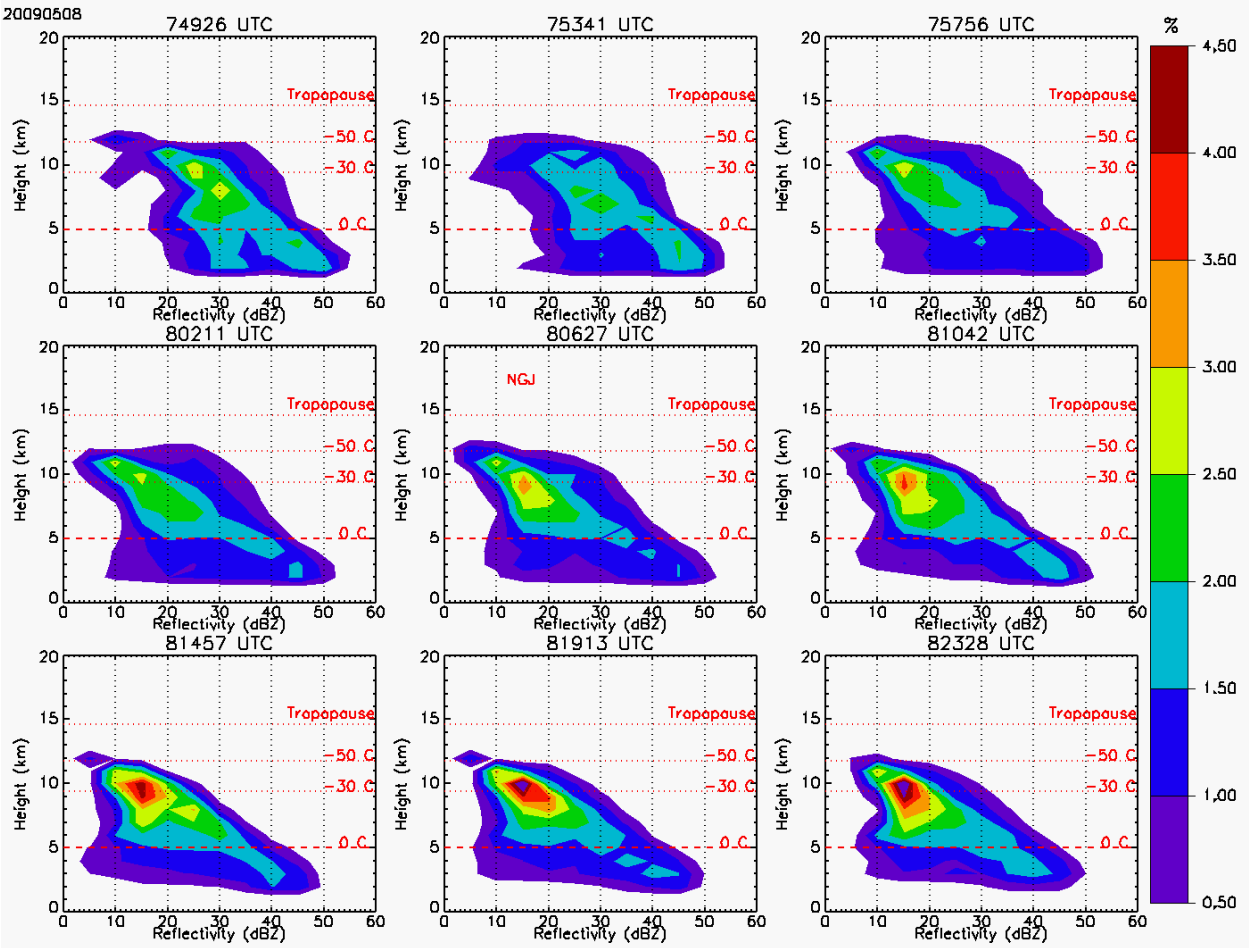

Figure 25. CFAD plots show the normalized distribution of reflectivity in 5 minute bins versus height for four time steps around the time of the jets. “GJ” is labeled in the diagrams when the jet occurred.

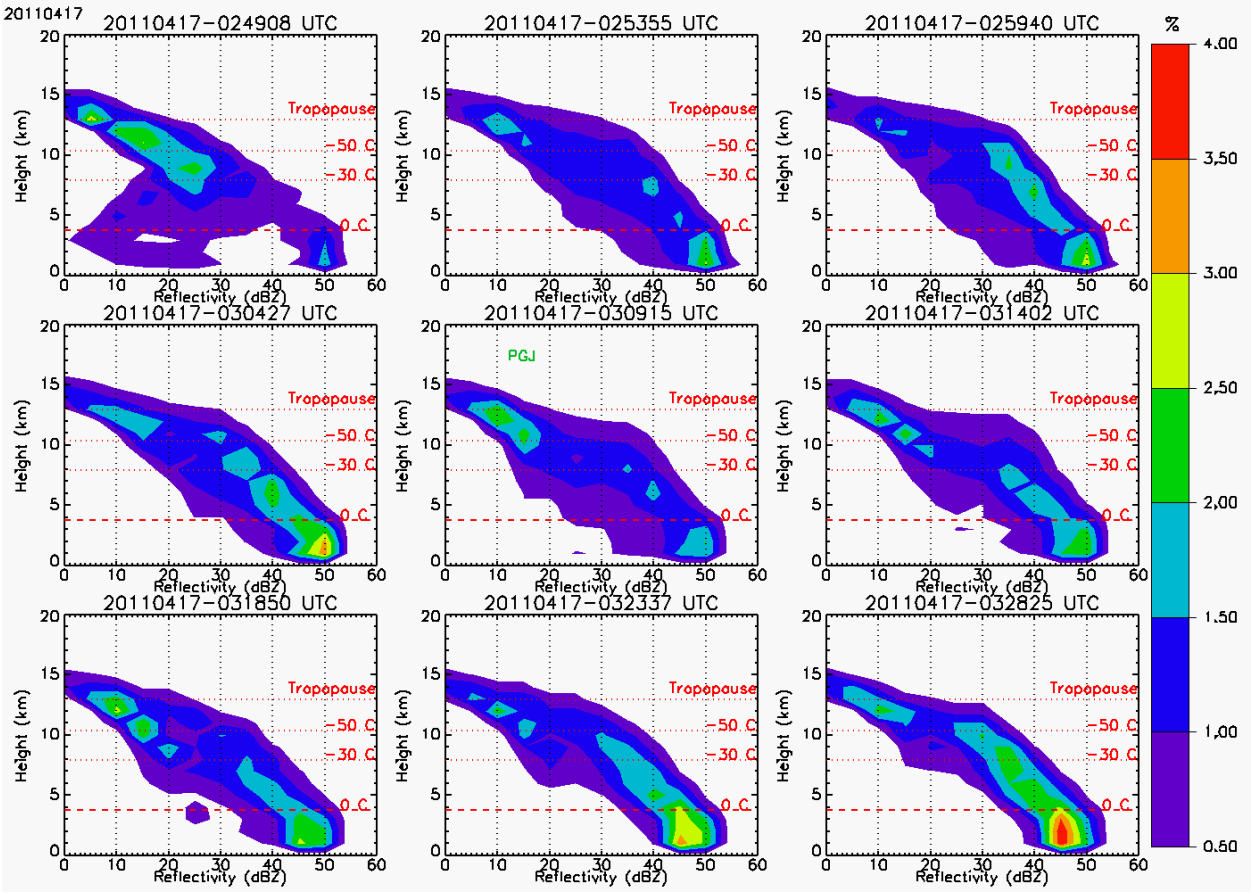

Figure 26. CFAD plots show the normalized distribution of reflectivity in 5 minute bins versus height for four time steps around the time of the jets. "GJ" is labeled in the diagrams when the jet occurred.

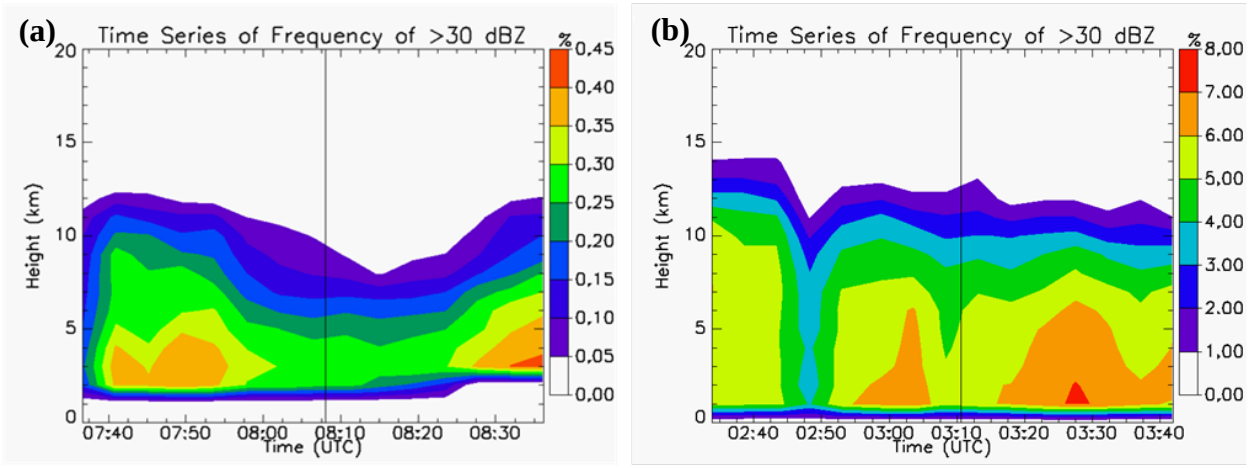

Figure 27. Time series plots of the frequency of >30 dBZ versus height in one km levels with the jet time denoted by the black vertical line for (a) 20090508 and (b) 20110417.

A time series of reflectivity for the 2009 negative GJ case shows similar results to the CFADs (Figure 27a). Unlike all the other cases, the reflectivity frequency in the upper levels was at a minimum at the time of the jet. There was also a minimum in lower level reflectivity

frequency around the time of the jet which was similar to the previous cases. The time series reflectivity for the 2011 positive GJ case shows a fairly flat reflectivity maximum except for a small peak within the 5 minutes after the time of the jet (Figure 27b).

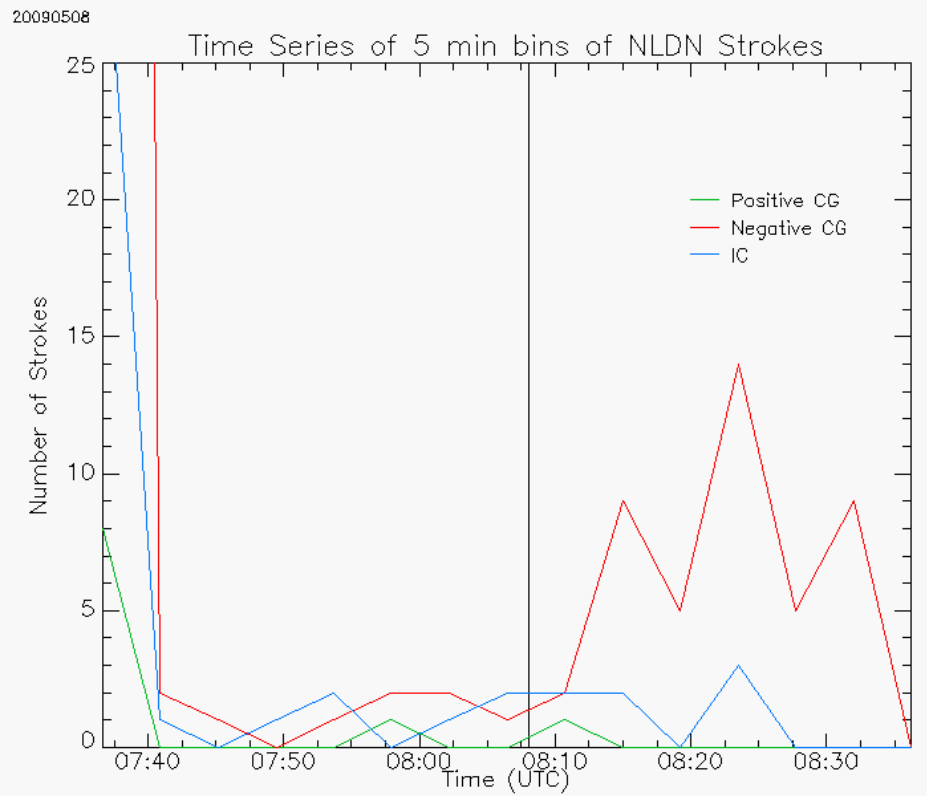

Figure 28. A time series plot of NLDN for lightning strokes in five minute bins versus height (one km levels). Positive CGs (green), negative CGs (red), IC (blue) are plotted with the time of the GJs (---).

The NLDN time series for the North Carolina cases are closer to the Puerto Rico case. The majority of the strokes were negative CGs and overall very little IC and positive CG lightning was noted. The 2009 negative GJ case had a lull in all lightning leading up to the time of the jet and then the negative CG lightning picked up after (Figure 28). This negative CG pattern is similar to that of the OK and FL cases. The positive jet case had peaks of negative CG lightning in the beginning of the storm and decreased after the jet occurred (Figure 29). Previous studies have suggested an inverted tripole established a vertical charge structure perhaps conducive to development of a positive jet, however the storm was still negative CG dominated.

There is simply not enough information to say that the structure was inverted or not, but the negative CG dominance could suggest it was a normal tripole structure. If this was the case, a new hypothesis would be needed to explain the formation of positive jets. There is simply not enough data to make any full conclusions about this.

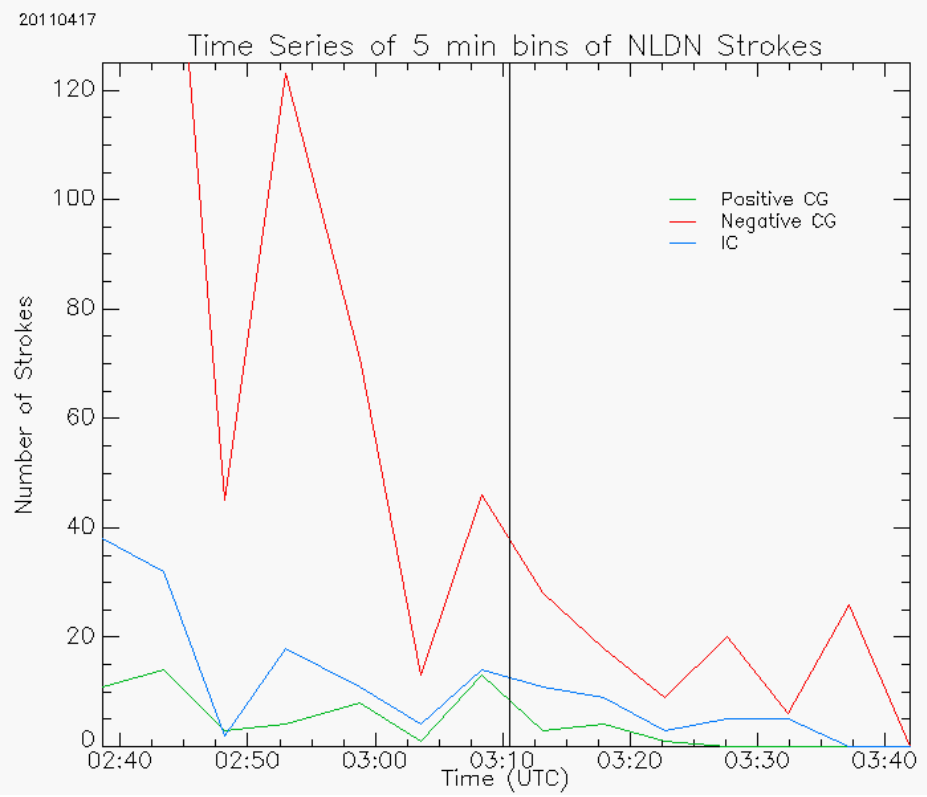

Figure 299. A time series plot of NLDN for lightning strokes in five minute bins versus height (one km levels). Positive CGs (green), negative CGs (red), IC (blue) are plotted with the time of the GJs (---).

The two North Carolina cases are outliers to the first 4 cases and previous studies. The negative jet formed in a storm that was at one of its weakest points and the positive jet was negative CG dominated. Both of these cases had lower melting level and tropopause heights as well as no obvious overshooting top.

4. Conclusions

The storm and lightning characteristics of six GJs have been examined. Table 2 shows a summary of these six cases along with some of their storm characteristics. Three of them were near very-high frequency LMAs. The Oklahoma case formed in remnants of Tropical Depression Hermine and contained a significant warm rain process, which may indicate why the maximum reflectivity was only 54-dBZ. The Florida, Puerto Rico, and North Carolina storms formed in environments with high CAPE and negative LI values which are good conditions for thunderstorm formation. The maximum reflectivity in the last four cases were 59-62 dBZ with 10-dBZ echo tops >14 km MSL. The Oklahoma and Puerto Rico GJs were located over land and the Florida and North Carolina cases were over water. The Oklahoma and Florida cases were marked by significant lightning-source frequency and upper-level reflectivity values associated with an overshooting top, indicative of a convective surge just prior to the GJ. The convective surge and normal polarity structure may have allowed the upper-positive charge to mix with the screening layer and become depleted. The IC lightning initiating in the mid-level negative region could have exited upward through the depleted positive charge region producing a negative jet reaching 80-90 km [*Lu et al*. 2011b]. According to *Krehbiel et al.* [2008], for a negative GJ to form from a normally electrified storm, it would need to originate in the mid-level negative storm charge. A discharge begins as a regular, upward-developing IC flash that causes a breakdown to occur allowing the leader to be of negative polarity resulting in a CG stroke that lowers negative charge to the ground. This leaves a charge imbalance where the upper positive charge is depleted. In the case of the GJ, the preferred discharge mode of the IC flash with a depleted upper positive charge is upward. For the Florida and Oklahoma case, the 3D lightning data can show that the storms are normally electrified along with the negative CG dominance.

The overshooting top and intensity of the storm at the time of the jet also suggests that mixing with the negatively charged screening layer may have also helped to further deplete the upper positive region. The Puerto Rico and North Carolina cases did not have as obvious of overshooting tops and the lightning data was limited to 2-D. However, it can be assumed they were normally electrified with their –CG dominance. Without an overshooting top, the negatively charged screening layer may not have been able to mix out, but the upper level positive region may have still been depleted enough. The negative North Carolina jet occurred as the lightning and reflectivity decreased and the storm weakened suggesting very little mixing aloft occurred. This is not consistent with the other cases and raises a question as to how the upper level positive region became depleted enough for the jet to occur. The –CG dominant storm was present in the positive North Carolina jet as well, suggesting a normal tripole structure of positive charge aloft, negative charge in the mid levels, and positive charge below. However this is puzzling for the positive GJ case since *Krehbiel et al.* [2008] suggests for a positive gigantic jet to form, a storm would be inverted. If this was not an inverted electrified storm, a new method would be needed to explain the formation. Since only 2-D lightning data were available, it cannot be confirmed whether this was or was not an inverted charged storm. If it was in fact normal polarity then a new method for gigantic jet formation would be needed to explain this. At this time, no hypotheses have been suggested; more positive jet cases need to be looked at to get a better understanding of the 3D lightning and storm structure.

Overall, the meteorological regime of six cases were looked to better understand the formation of gigantic jets and to see what types of storms they occur in. GJs have been observed in winter storms, squall lines, supercells, and tropical depressions. In order to make specific conclusions about the meteorological context of how GJs form more cases need to be looked at

within 3-D lightning arrays, but it is obvious the meteorological regimes here are distinctly different from those associated with most sprite producing convective systems [*Lyons et al*., 2009]. In more future work, with the new dual-polarized radars, it would be really interesting to look at the hydrometer type in the different regions and see how that plays a role in the type of lightning created.

Date	Time	Jet Type	Normal or Inverted	Overshooting Top?	Time of Max Refl	Max Refl (dBZ)	Hght of Max Refl (km)	CAPE (J/kg)	LI	Storm Top (km)
9 Sept 2010	72200	NGJ	Normal	Yes	71448	53.75	2	18-45	.27-2.6	16
	72820	NGJ		Yes						
28 Sept 2010	110120	NGJ	Normal	Yes	104103	58.88	2	2473	-4.8	17
22 Sept 2011	52706	NGJ	Normal	Maybe	52332	57.39	3	3500	-5.95	15
8 May 2009	80802	NGJ	Normal	No	75341	61.85	2	1207-118	-2.8-.4	14
17 April 2011	31128	PGJ	Normal?	Maybe	23933	62.15	2	2298	-6.4	16

5. References

Bering III, E.A., (1995), The global circuit: Global thermometer, weather by product or climate modulator? Rev. Geophys. 845-862 (supplement copy Part II),

Bering III, E.A., Few, A.A., Benbrook, J.R., (1998), The global electric circuit. Phys. Today 24-30 (Oct. issue),

Biagi, C.J., K.L. Cummins, K.E. Kehoe, and E.P. Krider, (2007), National Lightning Detection Network (NLDN) performance in southern Arizona, Texas, and Oklahoma in 2003-2004. *J. Geophys. Res.*, 112, doi:10.1029/2006JD007341.

Boyd, B. F., W. P. Roeder, D. Hajek, and M. B. Wilson, (2005), Installation, Upgrade, and Evaluation a Short Baseline Cloud-to-Ground Lightning Surveillance System in Support of Space Launch Operations, *1st Conference on Meteorological Applications of Lightning Data*, 9-13 Jan 05, 4 pp.

Carey, L.D., Rutledge, S.A., Petersen, W.A., 2003. The relationship between severe weather reports and cloud-to-ground lightning polarity in the contiguous United States from 1989 to 1998. Mon. Weather. Rev. 131, 1211 – 1228.

Cummer, S. A., et al. (2009), Quantification of the troposphere to ionosphere charge transfer in a gigantic jet, *Nat. Geosci., 2*, 617-620, doi:10.1038/ngeo607.

Cummins, K.L. and M.J. Murphy, (2009), An overview of lightning location systems: History, techniques, and data uses, with an in-depth look at the U.S. NLDN. IEEE Trans. On Electromagnetic Compatibility, Vol. 51, No. 3, 499-518.

Cummins KL, Krider EP, Malone MD (1998), The U.S. national lightning detection network and applications of cloud-to-ground lightning data by electric power utilities. *IEEE Transactions on Electromagnetic Compatibility* 40(4), 465–480.

Demetriades, N.W.S., M.J. Murphy, and J.A. Cramer, (2010), Validation of Vaisala's Global Lightning Dataset (GLD360) over the continental United States. Preprints, 29th Conf. Hurricanes and Tropical Meteorology, May 10-14, Tucson, AZ, 6 pp.

Glickman, T. S., (2000), Glossary of Meteorology. Amer. Meteor. Soc. 2nd Edition.

Holle, R. (2009), http://www.srh.noaa.gov/media/abq/sswhm/Holle_sw_hydromet_09.pdf.

Hondl, K. D., (2003), Capabilities and components of the Warning Decision Support System-Integrated Information (WDSS-II), Preprints, *19th Conf. on Interactive Information Processing Systems (IIPS) for Meteorology, Oceanography, and Hydrology*, Long Beach, CA, Amer. Meteor. Soc., CD-ROM, 14.7.

Hsu, R., et al. (2004), Transient luminous jets recorded in the Taiwan 2004 TLE campaign, *Eos Trans. AGU*, *85*(47), Fall Meet. Suppl., Abstract AW31a-0151.

Krehbiel, P. R., J. A. Riousset, V. P. Pasko, R. J. Thomas, W. Rison, M. A. Stanley, and H. E. Edens (2008), Upward electrical discharges from thunderstorms, *Nat. Geosci.*, *1*, 233-237, dio:10.1038/ngeo162.

Krehbiel et al., (2002), Three-dimensional total lightning observations with the lightning mapping array. *Int. Lightning Detection Conf*, 16–18 October 2002, Tucson, Vaisala, Tucson.

Krehbiel, P. R., R. J. Thomas, W. Rison, T. Hamlin, J. Harlin, and M. Davis, 2000: GPS-based mapping system reveals lightning inside storms. *Eos Trans. AGU*, 81(3), 21-21, 10.1029/00EO00014.

Krehbiel, P. R., (1986), The electrical structure of thunderstorms. The Earth's Electrical Environment, eds. E. P. Krider and R. G. Roble, Washington DC: National Academy Press., 90–113.

Kuhlman, K. M., Ziegler, C. L., Mansell, E. R., MacGorman, D. R., and Straka, J. M., (2006), Numerically simulated electrification and lightning of the 29 June 2000 STEPS supercell storm, 20 Mon. Wea. Rev., 134, 2734–2757.

Lakhina, G.S., (1993), Electrodynamic coupling between different regions of the atmosphere. Curr. Sci. 64, 660-666.

Lakshmanan, V., T. Smith, G. Stumpf, and K. Hondl. (2007), The Warning Decision Support System-Integrated Information. *Wea. And Forecasting*, 22, 596-612.

Lakshmanan, V., T. Smith, K. Hondl, G. J. Stumpf, and A. Witt, (2006), A real-time, three dimensional, rapidly updating, heterogeneous radar merger technique for reflectivity, velocity, and derived products. *Wea. Forecasting*, 21 (5), 802-823.

Lennon, C. and L. Maier, (1991), Lightning mapping system. 1991 Int'l. Aerospace and Ground Conf. on Lightning and Static Elec., NASA Conf. Pub. 3106, paper 89-1.

Lu, G., et al. (2011a), Analysis of lightning development associated with gigantic jets, American Geophysics Union (AGU) Fall Meeting Abstracts, AE13B-02, 2011 December, San Francisco, United States.

Lu, G., et al. (2011b), Lightning development associated with two negative gigantic jets, *Geophys. Res. Lett.*, *38*, L12801, doi:10.1029;2011GL047662.

Lyons, W.A., T.E. Nelson, R.A. Armstrong, V.P. Pasko, and M. A Stanley (2003), Upward electrical discharges from the tops of thunderstorms. Bull. Amer. Meteor. Soc., 84, 445-454.

Lyons, W.A., M.A. Stanley, J.D. Meyer, T.E. Nelson, S.A. Rutledge, T.L. Lang and S.A. Cummer, 2009: The meteorological and electrical structure of TLE-producing convective storms. In, Lightning: Principles, Instruments and Applications, H.D. Betz et al. (eds), 389-417 pp, Springer Science+Business Media B.V., doi: 10.1007/978-1-4020-9079-017.

MacGorman, D. R., et al. (2008), TELEX: The Thunderstorm Electrification and Lightning Experiment, Bull. Am. Meteorol. Soc., 89, 997–1013, doi:10.1175/2007BAMS2352.1.

MacGorman, D. R., and K. E. Nielsen, (1991), Cloud-to-ground lightning in a tornadic storm on 8 May 1986. *Mon. Wea. Rev.*,119, 1557–1574.

MacGorman, D. R., and W. D. Rust, The Electrical Nature of Storms, 422 pp., Oxford Univ. Press, New York, 1998

Maier, L., C. Lennon,T. Britt, and S. Schaefer, (1995), *LDAR system performance and analysis*, paper presented at International Conference on Cloud Physics, Am. Meteorol. Soc, Dallas, TX.

Marshall, T. C. et al., (2005), Observed electric fields associated with lightning initiation. *Geophys. Res. Lett.* 32, L03813.

Mohr, C. G., and R. L. Vaughn (1979), An economical approach for Cartesian interpolation and display of reflectivity factor data in three-dimensional space. *J. Appl. Meteor*., 18, 661–670.

Murphy, M. J., K. L. Cumins, N. W. S. Demetriades, and W. P. Roder (2008), Performance of the new Four-Dimensional Lightning Surveillance System (4DLSS) at the Kennedy Space Center/Cape Canaveral Air Force Station Complex, paper presented at 13th Conference on Aviation, Range, and Aerospace Meteorology, Am. Meteorol. Soc.,Boston, Mass.

Orville, R. E. (2008), Development of the national lightning detection network, Bull. Amer. Meteorol. Soc., 89(2), 180.

Orville, R.E. and G.R. Huffines, (2001), Cloud-to-ground lightning in the United States: NLDN results in the first decade, 1989-1998. *Mon. Wea. Rev.*,129, 1179-1193.

Pasko, V. P., and J. J. George (2002), Three-dimensional modeling of blue jets and blue starters, *J. Geophys., Res., 107*(A12), 1458, doi:10.1029/2002JA009473.

Pasko, V. P., M. A. Stanley, J. D. Mathews, U. S. Inan, and T. G. Wood (2002), Electrical discharge from a thundercloud top to the lower ionosphere, *Nature, 416*, 152-154, doi:10.1038/416152a.

Riousset, J. A., V. P. Pasko, P. R. Krehbiel, W. Rison, and M. A. Stanley (2010), Modeling of thundercloud screening charges: Implications for blue and gigantic jets, J. Geophys. Res., 115, A00E10, doi:10.1029/2009JA014286.

Roble, R.G., (1991), On modeling component processes in the earth's global electric circuit. J. Atmos. Sol.-Terr. Phys. 53, 831-847.

Roble, R.G., Tzur, I., (1986), The global atmospheric electrical circuit. Study in Geophysics--The Earth's Electrical Environment. National Academy Press, Washington, D.C., pp. 206-231.

Roeder, W. P. (2010), The four dimensional lightning surveillance system, paper presented at 21st International Lightning Detection Conference, Vaisala, Orlando, Fla.

Rycroft, M.J., Israelsson, S., Price, C., (2000), The global atmospheric electric circuit, solar activity and climate change. J. Atmos. Sol.-Terr. Phys. 62, 1563-1576.

Said, R. K., U. S. Inan, and K. L. Cummins (2010), Long-range lightning geo-location using a VLF radio atmospheric waveform bank, J. Geophys.Res., 115, D23108, doi:10.1029/2010JD013863.

Siingh, Devendraa, Singh, R.P., Kamra, A.K., Gupta, P.N., Singh, R., Gopalakrishnan, V., Singh, A.K., (2005), Review of electromagnetic coupling between the Earth's atmosphere and the space environment. J. Atmos. Sol.-Terr. Phys. 67, 637-658.

Soula, S., O. van der Velde, J. Montanya, P. Huet, C. Barthe, and J. Bór (2011), Gigantic jets produced by an isolated tropical thunderstorm near Réunion Island, J. Geophys. Res., 116, D19103, doi:10.1029/2010JD015581.

Su, H.T., et al. (2003), Gigantic jets between a thundercloud and the ionosphere, *Nature*, *423*, 974-976, doi:10.1038/nature01759.

Thompson, W., (1860), in *Nichols Cyclopedia*, Nichols, London.

Vailsala Inc. (2011), Vaisala's NLDN® U.S. National Lightning Detection Network®.

van der Velde, O. A., W. A. Lyons, T. E. Nelson, S. A. Cummer, J. Li, and J. Bunnell (2010), Multi-instrumental observations of a positive gigantic jet produced by a winter thunderstorm in Europe, *J. Geophys. Res.*, *115*, D24301, doi:10.1029/2010JD014442.

van der Velde, O. A., et al. (2007a), Analysis of the first gigantic jet recorded over continental North America, *J. Geophys. Res., 112*, D20104, doi:10.1029/2007JD008575.

van der Velde, W.A. Lyons, S.A. Cummer, N. Jaugey, D.D. Sentman, M.B. Cohen and R. Smedley (2007b), Electromagnetic, visual and meteorological analyses of two gigantic jets observed over Missouri. Eos Trans AGU, Fall Meet, Suppl., Poster, Abstract AE23A-0895.

Weins, K. C., Rutledge, S. A. & Tessendorf, S. A. (2005), The 29 June 2000 supercell observed during STEPS. Part II: Lightning and charge structure. J. Atmos. Sci. 62, 4151-4177.

Wescott, E. M., Stenbaek-Nielsen, H. C., Huet, P., Heavner, M. J. & Moudry, D. R., (2001), New evidence for the brightness and ionization of blue jets and blue starters. *J. Geophys. Res.* 106, 21549–21554.

Wescott, E. M., Sentman, D. D., Heavner, M. J., Hampton, D. L. & Vaughan, O. H.Jr., (1998), Blue jets: Their relationship to lightning and very large hailfall, and their physical mechanisms for their production. *J. Atmos. Sol. Terr. Phys.* 60, 713–724.

Williams, E.R., et al. (1999), The behavior of total lightning activity in severe Florida thunderstorms. *Atmos. Res.,* 51, 245–264.

Williams, E. R., (1989), The tripolar structure of thunderstorms. *J. Geophys. Res.* 94, 13151–13167.

Williams, E. R., M. E. Weber, and R. E. Orville, (1989), The relationship between lightning type and convective state of thunderclouds. *J. Geophys. Res.*, 94, 213–220.

Wilson, C. T. R., (1956), A theory of thundercloud electricity. *Proc. R. Soc. Lond. A*236, 297–317.

Wilson, C. T. R., (1921), Investigations on lightning discharges and on the electric field of thunderstorms. *Phil. Trans. R. Soc. Lond. A* 221, 73–115.

Yuter, S. E., and R. A. Houze Jr. (1995), Three-dimensional kinematic and microphysical evolution of Florida cumulonimbus. Part II: Frequency distribution of vertical velocity, reflectivity, and differential reflectivity. *Mon. Wea. Rev.*, 123, 1941–1963.